PŘÍRODOVĚDECKÁ
FAKULTA
Univerzita Karlova

DIPLOMOVÁ PRÁCE

Ondřej Groborz

Pharmacokinetics of Intramuscularly Administered Thermoresponsive Polyacrylamides

Farmakokinetika intramuskulárně aplikovaných termoresponsivních polyakrylamidů

Vedoucí práce: doc. Mgr. Martin Hrubý, Ph.D., DSc.

Konzultanti: Ing. Pavel Švec
RNDr. Lenka Loukotová, Ph.D.

Studijní program: Chemie

Studijní obor: Medicinální chemie

Praha
2021

Prohlašuji, že jsem tuto diplomovou práci vypracoval samostatně a výhradně s použitím citovaných pramenů, literatury, dokumentace přístrojů a dalších odborných zdrojů. Při jejím vypracovávání byla použitá data získaná mnou nebo mými kolegy.

Prohlašuji, že jsem tuto práci ani žádnou její podstatnou část nepředložil k získání jiného či stejného akademického titulu.

V Praze dne Ondřej Groborz

Poděkování

Chtěl bych poděkovat velké řadě spoluautorů, bez nichž by tato práce nemohla vzniknout. Mé velké poděkování patří Ing. Kristýně Kolouchové, Ph.D., Ing. Pavlu Švecovi, a RNDr. Lence Loukotové, Ph.D. za jejich cenné rady, předané zkušenosti, podporu, pomoc s návrhy a provedením experimentů a jejich částečné financování.

Dále bych chtěl poděkovat Mgr. Janu Pankrácovi a Ing. Peteru Kešovi, Ph.D. za pomoc s designem a realizací biologických experimentů. Hodně mi pomohl také Mgr. Volodymyr Lobaz, Ph.D. a Ing. Hynek Beneš, Ph.D. s měřením interpretace kalorimetrických experimentů; Mgr. David Babuka s měřením a vyhodnocením DLS. Velké poděkování si také zaslouží MSc. Jan Kadlec, který mi pomáhal s odvozováním farmakokinetických modelů a zpracováním dat. Rád bych poděkoval MVDr. Anetě Pierzynové, MUDr. Jaromíru Šrámkovi, RNDr. Márii Hovořákové, Ph.D., Mgr. Lindě Dalecké a doc. MUDr. Tomáši Kučerovi, Ph.D. za rozsáhlou pomoc s histopatologickým vyšetřením zvířat a za interpretaci výsledků. Na závěr děkuji RNDr. Petru Štěpánkovi, DrSc., prof. Richardu Hoogenboomovi, Ph.D., RNDr. Luďku Šefcovi, Ph.D., a doc. Mgr. Martinu Hrubému, DSc. za podporu, konzultace výsledků a přístupu k požadovaným přístrojům a technice. Chtěl bych také poděkovat Dr. Carlosu V. Melovi za cenné rady, editace manuskriptu a revize obsahu.

Bylo mi velkou ctí s nimi spolupracovat. Svou pomocí, radami a upomínkami umožnili vznik této práce, za což jsem jim velmi vděčný. Děkuji i všem ostatním, všem přátelům, rodině, kolegům, učitelům a dalším, kteří mě jakkoliv podporovali, poučili, inspirovali a měli se mnou trpělivost, i když se nejednalo zrovna o kontext této práce.

Tato práce byla spolufinancována Grantovou Agenturou Univerzity Karlovy (GAUK, projekt 379321).

Acknowledgement

I would like to acknowledge a great help of Ing. Kristýna Kolouchová, Ph.D., Ing. Pavel Švec, and RNDr. Lenka Loukotová, Ph.D. for their valuable advice, expertise, support, help with experiments planning and performance and the financial support.

Then, I would like to thank Mgr. Jan Pankrác, and Ing. Peter Keša, Ph.D. for their help with biological experiment design and performance. Mgr. Volodymyr Lobaz, Ph.D. and Ing. Hynek Beneš, Ph.D. have helped me with calorimetric experiments and the results interpretation; Mgr. David Babuka helped with DLS measurement, processing and its interpretation.

I would like to express my gratitude to MVDr. Aneta Pierzynová, MUDr. Jaromír Šrámek, RNDr. Mária Hovořáková Ph.D., Mgr. Linda Dalecká, and doc. MUDr. Tomáš Kučera, Ph.D. for their help with histopathological examination of the animals yand the results interpretation. My gratitude belongs to MSc. Jan Kadlec for his help with pharmacological model evaluation and the data interpretation. Lastly, I would like to acknowledge the help from RNDr. Petr Štěpánek, DrSc., prof. Richard Hoogenboom, Ph.D., RNDr. Luděk Šefc, Ph.D., and doc. Mgr. Martin Hrubý, DSc. for their support, results consultation and providing access to the required instruments. I would also like to thank Dr. Carlos V. Melo for editing parts of the manuscript and reviewing the content.

It has been an honour to work with them. Their help and advice were incredibly useful, and I am very grateful for them. I would like to thank everyone else, all friends of mine, my family, my colleagues, my teachers, *etc*. who have supported me in any way, edified me, inspired me, or had patience with me, even if they were not directly connected to this thesis.

The authors gratefully acknowledge the funding from the Grant Agency of Charles University, GA UK (Project No. 379321).

Farmakokinetika intramuskulárně aplikovaných termoresponzivních polyakrylamidů

Autor: Ondřej Groborz

Vedoucí práce: doc. Mgr. Martin Hrubý, Ph.D., DSc.
Ústav makromolekulární chemie,
Akademie věd České republiky

Konzultanti: Ing. Pavel Švec
RNDr. Lenka Loukotová, PhD.

Abstrakt

Roztoky některých polymerů vykazují dolní kritickou rozpouštěcí teplotu (lower critical solution temperature, LCST). Takové polymery za určitých podmínek vytvářejí homogenní roztoky, ale jakmile teplota roztoku překročí kritickou teplotu (cloud point temperature, T_{CP}), dojde k fázové separaci. Pro tyto polymery bylo navrženo nespočet aplikací v rámci medicinální chemie a medicíny, například *in situ* formovaná depa pro radioterapii (brachytherapii), *in situ* formovaná depa pro protrahované uvolňování léčiv, imunoradiotherapie, injekční thermogelling pro tkáňová inženýrství a pěstování buněčných kultur, tracery pro magnetickou rezonanci (MRI) a mnoho dalších. Navzdory četným navrženým využitím a rozsáhlému výzkumu těchto polymerů, farmakokinetika injekovaných termoresponzivních polymerů stále není dostatečně dobře prozkoumána.

V této práci se věnujeme syntéze a důkladné fyzikálně-chemické charakterizaci čtyř různých termoresponzivních polyakrylamidů, konkrétně poly(*N*-(2,2-difluoroethyl)akrylamidu, poly(*N*-isopropylakrylamidu), poly(*N*,*N*-diethylakrylamidu), a poly(*N*-akryloylpyrrolidinu) za fyziologicky relevantních podmínek. Následně sledujeme biodistribuci a farmakokinetiku těchto polymerů v myším modelu po intramuskulárním podání. Na základě získaných dat navrhneme fyziologický model pro farmakokinetiku a hledáme korelace různých fyzikálně-chemických parametrů polymerů s pozorovanou farmakokinetikou a *in vitro* chováním. Naše závěry je možné použít k návrhu polymerů s definovanou farmakokinetikou pro zvolené medicinálně chemické aplikace.

Klíčová slova: polyakrylamidy, thermoresponzivní, farmakokinetika, *in vivo*, polymery, biodistribuce, fluorescence

Pharmacokinetics of Intramuscularly Administered Thermoresponsive Polyacrylamides

Author: Ondřej Groborz

Supervisor: doc. Mgr. Martin Hrubý, Ph.D., DSc.
Institute of Macromolecular Chemistry,
Czech Academy of Sciences

Advisers: Ing. Pavel Švec
RNDr. Lenka Loukotová, PhD.

Abstract

Polymer solutions with lower critical solution temperature (LCST) undergo a phase separation when heated above their cloud point temperature (T_{CP}). These thermoresponsive polymers have numerous promising medicinal applications, such as *in situ* depot-forming radiotherapy (brachytherapy), controlled drug-release, immuno-radiotherapy, injectable thermogelling for tissue engineering and cell culture and magnetic resonance imaging (MRI), among others. Yet, despite extensive research on medicinal applications of thermoresponsive polymers, their fate after their administration remains largely unknown.

Thus, in our study, we synthesized and thoroughly characterized four different thermoresponsive polyacrylamides, namely poly(*N*-(2,2-difluoroethyl)acrylamide), poly(*N*-isopropylacrylamide), poly(*N*,*N*-diethylacrylamide) and poly(*N*-acryloylpyrrolidine) under physiologically relevant conditions. Subsequently, we determined their biodistribution kinetics in mice and proposed a data-based pharmacological model to describe their *in vivo* behaviour, correlating their physico-chemical properties with their pharmacokinetics. Overall, our findings may be used to tailor their properties to meet the demands of their medicinal applications.

Key words: polyacrylamides, thermoresponsive, pharmacokinetics, *in vivo*, polymers, biodistribution, fluorescence

Prohlášení o autorství

Tato práce obsahuje data, interpretace a formulace, které byly/budou použity v publikacích:

(1) Kolouchová K., Lobaz V., Beneš H., Rosa V.R., Babuka D., Švec P., Černoch P., Hrubý M., Hoogenboom, R., Štěpánek P., **Groborz O.**; *Thermoresponsive Properties of Polyacrylamides in Physiological Solutions*, Polymer Chemistry, v revizi, přijato **8/2021,** DOI: 10.1039/d1py00843a

(2) **Groborz O.**, Kolouchová K., Pankrác J., Keša P., Kadlec J., Krunclová T., Pierzynová A., Šrámek J., Hovořáková M., Dalecká L., Kučera T., Švec P., Loukotová L. Hoogenboom R., Hrubý M.; *Pharmacokinetics of Intramuscularly Administered Thermoresponsive Polyacrylamides*, článek v přípravě

Authorship declaration

This thesis contains data, interpretations, and formulations which were/ will be used in following publications:

(1) Kolouchová K., Lobaz V., Beneš H., Rosa V. R., Babuka D., Švec P., Černoch P., Hrubý M., Hoogenboom, R., Štěpánek P., **Groborz O.**; *Thermoresponsive Properties of Polyacrylamides in Physiological Solutions*, Polymer Chemistry, in revision, accepted **8/2021,** DOI: 10.1039/d1py00843a

(2) **Groborz O.**, Kolouchová K., Pankrác J., Keša P., Kadlec J., Krunclová T., Pierzynová A., Šrámek J., Hovořáková M., Dalecká L., Kučera T., Švec P., Loukotová L. Hoogenboom R., Hrubý M.; *Pharmacokinetics of Intramuscularly Administered Thermoresponsive Polyacrylamides*, manuscript in preparation

Konflikty zájmu

O. Groborz vlastní akcie firmy Bausch Health Companies Inc. (Laval, Kanada). Její dceřiná firma (Bausch + Lomb, Laval, Kanada) vyrábí gel Visidic®, který byl použit v této studii. Žádná firma, poskytovatel grantu, ani zaměstnavatel neovlivňovali provedení studie, její vyhodnocení ani závěry této práce.

Conflicts of interests

O. Groborz is a stockholder of Bausch Health Companies Inc. (Laval, Canada). Its subsidiary, Bausch + Lomb (Laval, Canada) licences Visidic® gel, which was used in this study. No company, grant agency or employer influenced the design of the stury, its evaluation, nor its conclusions.

List of used abbreviations and symbols

Abbreviation	Explanation (base unit)
^{1}H NMR	^{1}H nuclear magnetic resonance
^{1}H MRI	^{1}H magnetic resonance imaging
^{1}H-^{13}C HSQC-edit NMR	^{1}H-^{13}C multiplicity edited, heteronuclear single quantum coherence spectroscopy nuclear magnetic resonance
^{13}C{^{1}H} NMR	^{13}C nuclear magnetic resonance with ^{1}H decoupling
^{19}F NMR	^{19}F nuclear magnetic resonance
A	fraction of the administered polymer which becomes tissue bound (enters the Phase 2 of the kinetics)
ACVA	4,4'-[(E)-diazenediyl]bis(4-cyanopentanoic acid)
AIBN	2,2′-azobis(2-methylpropionitrile)
ANOVA	analysis of variance
B	overall magnetic field (T)
B_0	external magnetic field (T)
B_{shiled}	magnetic field from the local electron movements (T)
BPO	dibenzoyl peroxide
c_x	molar concentration of compound x (mol·L^{-1})
CI	confidence interval
CI_{90}	confidence interval, 90%
CI_{95}	confidence interval, 95%
CI_{99}	confidence interval, 99%
CPT	cloud point temperature
CTA	chain transfer agent
CA	California, state of the USA
D	diffusion coefficient (diffusivity, or mass diffusivity)
D	content of deuterium of all hydrogen atoms (*e.g.* 'in 99.80% D')
d	doublet (in NMR)
dd	doublet of doublets (in NMR)
ddd	doublet of doublets of doublets (in NMR)
DEPT	distortionless enhancement by polarization transfer
dn/dc	specific refractive index increment (L·g^{-1})
DLS	dynamic light scattering
DMEM	Dulbecco modified Eagle medium

DMF	*N*,*N*-dimethylformamide
DSC	differential scanning calorimetry
DMSO	dimethyl sulfoxide
DMSO-6d	perdeuterated dimethyl sulfoxide
DYE-NH_2	amino-derivative of a fluorescent dye (in this case Cy7-amine)
$\boldsymbol{e}$	Euler's number (≈ 2.718)
E₁	poly[(*N*,*N*-diethyl)acrylamide], lowest M_w
E₂	poly[(*N*,*N*-diethyl)acrylamide], medium M_w
E₃	poly[(*N*,*N*-diethyl)acrylamide], highest M_w
F₁	poly[(*N*-2,2-difluoroethyl)acrylamide], lowest M_w
F₂	poly[(*N*-2,2-difluoroethyl)acrylamide], medium M_w
F₃	poly[(*N*-2,2-difluoroethyl)acrylamide], highest M_w
FBS	foetal bovine serum (fetal bovine serum in US English)
GA UK	Grantová agentura UK (the Charles University Grant Agency)
GPC	gel permeation chromatography
H&E	haematoxylin & eosin stain
HF	human fibroblasts
HPLC	high-performance liquid chromatography
HSQC	heteronuclear single quantum coherence spectroscopy
I_R	intensity of signal in fluorescence imaging
I₁	poly[(*N*-isopropyl)acrylamide], lowest M_w (see **Table 1**)
I₂	poly[(*N*-isopropyl)acrylamide], medium M_w (see **Table 1**)
I₃	poly[(*N*-isopropyl)acrylamide], highest M_w (see **Table 1**)
IR-A	infrared light, subtype A (700 to 1400 nm)
IR-B	infrared light, subtype B (1400 to 3000 nm)
IR-C	infrared light, subtype C (3000 to 10.000.000 nm)
ITC	isothermal titration calorimetry
J	spin-spin coupling constant (J-coupling constant)
k	kinetics constant (s^{-1})
$k_{NTB\rightarrow B}$	dissolution constant of the non-tissue bound polymer
$k_{TB\rightarrow B}$	dissolution constant of the tissue bound polymer
k_{KID}	dissolution constant of the kidney depot
k_{LIV}	dissolution constant of the liver depot

LCST	lower critical solution temperature
LFT	lattice fluid theory
LFT-HB	lattice fluid theory with hydrogen bonding correction
NMR	nuclear magnetic resonance
m	multiplet (in NMR)
m_x	mass of compound x (kg)
M_n	number-average molar mass ($g \cdot mol^{-1}$)
M_w	weight-average molecular weight ($g \cdot mol^{-1}$)
MALS	multiangle light scattering
MeOH	methanol
MeOH-4d	perdeuterated methanol
MiliQ/MilliQ water	ultrapure water
MRI	magnetic resonance imaging
n	refractive index
n'	sample size
n_x	molar amount of compound x (mol)
N	number of energy states
N_0	population of low spin state
N_1	population of high spin state
$PrNH_2$	propylamine
n/a	not applicable
N/A	not available
p	p-value
P1	poly[(*N*-acryloyl)pyrrolidine], lowest M_w
P2	poly[(*N*-acryloyl)pyrrolidine], medium M_w
P3	poly[(*N*-acryloyl)pyrrolidine], highest M_w
PAI	photoacoustic imaging
pAP	poly[(*N*-acryloyl)pyrrolidine
PBS	phosphate saline buffer
PDI	dispersity index ($Đ = M_n/M_w$)
pDFEA	poly[(*N*-2,2-difluoroethyl)acrylamide]
pDEA	poly[(*N*,*N*-diethyl)acrylamide]
PET	positron emission tomography

pH	potential of hydrogen
pNIPAM	poly[(*N*-isopropyl)acrylamide]
ppm	parts per million
PyBOP	(benzotriazol-1-yloxy)tripyrrolidinophosphonium hexafluorophosphate
R_h	hydrodynamic radius of the particle (m)
RI	refractive index
rMSC	rat mesenchymal stem cells
ROI	region of interest
rpm	revolutions per minute; rotations per minute
RAFT	reversible addition−fragmentation chain-transfer polymerization
S	spin quantum number
S_R	area of depot in fluorescence imaging
SAXS	small-angle X-ray scattering
SD	standard deviation
SEC	size exclusion chromatography
SI	supporting information
SPECT	single photon emission computer tomography
t	triplet (in NMR)
T	temperature (K)
T_1	spin–lattice relaxation time (s)
$t_{½}$	half-life of nuclide or reaction (s)
T_{CP}	cloud point temperature (K)
TCEP	tris(2-carboxyethyl)phosphine hydrochloride
TEA	triethylamine
TGC	time gain compensation
THF	tetrahydrofuran; oxolane
tt	triplet of triplets (in NMR)
tdd	triplet of doublets of doublet (in NMR)
UCST	upper critical solution temperature
US	ultrasound
US-PAI	ultrasound-photoacoustic imaging
UV	ultraviolet [light]

UV/VIS	ultraviolet/visible light
UV-A	ultraviolet light, subtype A (315 to 400 nm)
UV-B	ultraviolet light, subtype B (280 to 315 nm)
UV-C	ultraviolet light, subtype C (100 to 218 nm)
V_x	volume of compound x (L)
v/v	volume fraction, volume per volume
WAXS	wide-angle X-ray scattering
$\overline{x}$	mean value
z_y	confidence level value (z_{90} = 1.645, z_{95} = 1.96, z_{99} = 2.576)
γ	gyromagnetic ratio (rad·s^{-1}·T^{-1})
δ	chemical shift factor
δ_{sample}	chemical shift of the study atom
η	viscosity of the media (kg·m·s^{-2})
ΔE	energies between the two energetic states (J·mol^{-1})
ΔH	change of enthalpy (J·mol^{-1})
λ	wavelength (m^{-1})
π	constant, ≈ 3.14159
τ	delay time (s)
ω	angular frequency (Larmor frequency; rad·s^{-1})
ω_{sample}	Larmor frequency of the study atom (rad·s^{-1})
ω_{ref}	Larmor frequency of a reference atom (rad·s^{-1})
$Đ_M$	dispersity index, defined as M_w/M_n
$\hbar$	reduced Planck's constant (Dirac constant; ≈ 1.055·10^{-34} J·s)

Table of content

1. Introduction

1.1. Polymer synthesis

Numerous synthetic approaches can be employed to prepare polymers with a narrow molar weight distribution (low dispersity, $Đ_M$). Probably the most common method of preparing polymers with a low polydispersity is the living polymerization with fast rate of initiation.[3,4] In these methods, the growing polymer chain is stabilized with a moiety, that enables the addition of new monomer units, but prevents the chain depolymerization and growth termination. As a result, if the polymerization is initialized quickly, all polymer chains have nearly equal lengths (because they grow statistically, and their growth cannot be terminated).

A very convenient polymer preparation method is the reversible-deactivation radical polymerization (RAFT) synthesis (**Figure 1**), which is a type of the living polymerization. This synthesis occurs in three steps:[5]

Step I: **initiation**. The reaction is most often initialized by *in situ* generated reactive radical species, which can be conveniently accomplished with heat-induced/ photoinduced degradation of 2,2′-azobis(2-methylpropionitrile) (AIBN), dibenzoyl peroxide (BPO), 4,4'-azobis(4-cyanopentanoic acid) (AVPA), or similar compounds.[5]

Step II: **propagation**. The *in situ* generated radicals react with monomer forming an oligomer/polymer chain with an unpaired valence electron at its end, which can be stabilized by RAFT-reagent. Note, that the stabilization with RAFT-reagent is reversible under the reaction conditions, therefore, the stabilized (non-reactive) radical RAFT-protected polymer chain can convert back into the more reactive non-protected polymer chain, which can continue the polymer propagation. In ideal conditions, the unpaired electron is never recombined or transformed in an irreversible reaction, thus the polymer chain growth should continue until uninterrupted by quenching reactions.[5]

Step III: **quenching (termination)**. At a predetermined timepoint, a new reagent (usually water, alcohols, or amines) is added into the reaction flask, thereby terminating the polymer growth. If performed correctly, RAFT-reaction provides a polymer product with a defined polymer length and low dispersity index (as low as 1.05 or lower).[5]

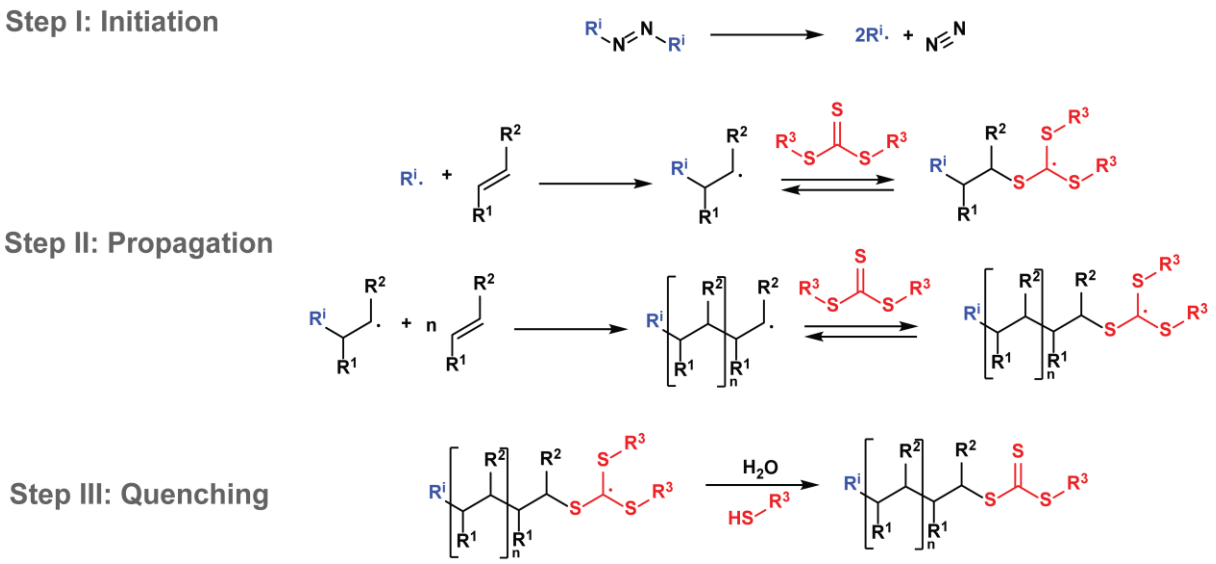

Figure 1. The general scheme of RAFT polymer synthesis.[5]

1.2. Thermoresponsive polymers

Thermoresponsive (temperature-responsive) polymers are those polymers, whose physico-chemical properties change discontinuously with the change of temperature. Most commonly, the concerned property is the solubility of these polymers in a solvent. In principle, we can distinguish two types of thermoresponsiveness of solutions: lower critical solution temperature (LCST) and upper critical solution temperature (UCST; **Figure 2**). LCST-type of thermoresponsive solutions form homogeneous solutions **below** a threshold temperature (cloud point temperature, T_{CP}) but separate into two phases with high and low concentrations upon heating above this T_{CP}.[5] UCST-type of thermoresponsive solutions form homogeneous solutions **above** a threshold temperature (T_{CP}), but separate into two phases with high and low concentrations upon cooling below this T_{CP}.[6]

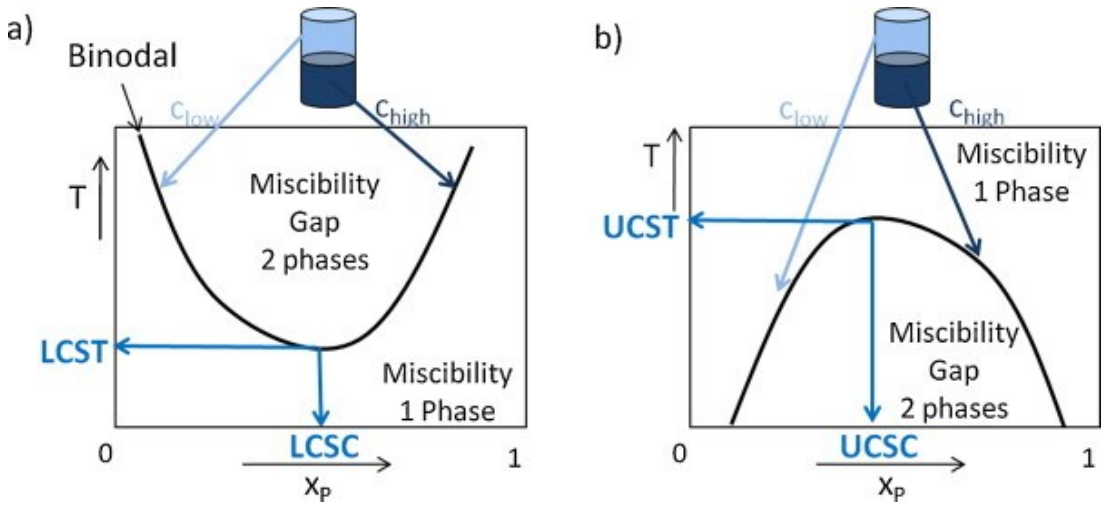

Figure 2. Phase diagram for a binary polymer–solvent mixture exhibiting (**A**) LCST behaviour and (**B**) UCST behaviour; adapted from literature.[7]

T_{CP} depends on polymer molar mass (dispersity)[6,8–11] and concentration,[6,8,12] on solution pH[13–16] and on the concentration and type of ions[16–24] (due to the Hofmeister effect[17]), proteins and other macromolecules[16,25–28] in solution (due to the excluded volume/ molecular crowding effect,[29] competition for solvent, or non-covalent protein-polymer interactions[30]), among other factors.[6,9,31] Polymer tacticity[6,32] and terminal moiety (*e.g.*, a chain transfer agent, CTA)[6,33,34] and even fairly subtle environmental changes, including changes in solution pH,[15,23,35] can also affect the T_{CP}. Several theories, especially the Lattice Fluid Theory with hydrogen-bonding corrections (LFT-HB)[36] and other (more advanced) models,[28,37–40] reliably describe T_{CP} as a function of polymer concentration but they are rather complicated and heavily rely on empirical data.[28,36–40] Unsurprisingly, many authors agree with the need to assess the thermoresponsive properties of a polymer experimentally.[8,9,17,19,28,37,41]

Many techniques can be used to determine the T_{CP} of a given polymeric system, such as turbidimetry/ spectrophotometry, rheology, refractometry, infrared spectroscopy, small-angle neutron scattering, dynamic light scattering and small-angle/-wide angle X-ray scattering (DLS, SAXS WAXS), ^{1}H or ^{19}F NMR (nuclear magnetic resonance) spectroscopy, isothermal and differential scanning (micro)calorimetry, among others. Spectrophotometry (turbidimetry) is arguably the most common method for determining the T_{CP} of a solution of a thermoresponsive polymer because this method is widely available, quick, sensitive, and robust, accurately providing the T_{CP} at both high and relatively low concentrations. However, beam wavelength,[42] heating and stirring rates,[42,43] as well as the selected threshold absorbance,[8,42] can alter the measurement sensitivity and thus shift the experimental T_{CP}.[42] Moreover, this method may be inaccurate for absorbing (coloured) or non-homogeneous samples[15,42] and for polymer solutions with a very low refractive index increment (dn/dc) – for such samples, DLS is a more reliable option.[42] In turn, DLS may provide additional information about the variation in the size of molecular assemblies as a function of temperature (with some bias concerning larger structures),[44] but this method is more time demanding and laborious than turbidimetry.[44]

Notwithstanding the wide range of methods for determining the T_{CP} of thermoresponsive polymers and for their thorough characterization, most previous systematic studies have only done so in non-physiological solutions. Furthermore, the solvent (phosphate-buffered saline, PBS, foetal bovine serum, FBS, plasma, serum, and interstitial fluid) effect on the T_{CP}s of such polymer solutions has never been systematically assessed, with most researchers analysing the effects of polymer molar weight or salts/ proteins on T_{CP} separately and under different conditions. Similar homopolymers prepared/ measured under different conditions may display

vastly different thermoresponsive properties, as shown by meta-analysis.[6,8] Therefore, understanding how molar mass and salts/ proteins affect T_{CP} requires assessing all these effects with one batch of polymers in a head-to-head study. While numerous thermoresponsive homopolymers have already been reported, out of polyacrylamides, only poly[(*N*-isopropyl)acrylamide] (**pNIPAM**)[16–20,26,27,45,46] and poly[(*N*-acryloyl)pyrrolidine] (**pAP**)[20] have been extensively studied in both water and (at least partly) physiologically relevant solutions. Those studies have shown that T_{CP} is significantly lower in those solutions than in water.

1.3. Applications of thermoresponsive polymers

Thermoresponsive polymers have been proposed/ investigated for many (biomedical) applications. An example of a promising biomedical application is the *in vivo* formation injectable implants/ depots (**Figure 3**).[13,47] In this applications, non-toxic thermoresponsive (co)polymers with T_{CP} bellow body temperature are dissolved in water at room temperature and administered into a target tissue. Upon administration, the solution heats up to body temperature and therefore forms a physically cross-linked aggregates, which can be used *e.g.* in wound dressing.[48,49] If a hydrophobic drug is *co*-administered with the polymer, the drug becomes "trapped" in the polymer aggregates, which can substantially prolong the release of the drug into the surrounding tissue and thus prolonging its effect.[13,47,50–52] Furthermore, thermoresponsive polymers can be labelled with radioactive nuclides and used for brachytherapy.[53,54] Thermoresponsive polymers have been proposed and investigated across various fields, including switchable substrates for cell/tissue culture,[55–58] drug delivery systems,[59,50] gene delivery/therapy[60–62], tissue engineering,[57,63–65] wound dressing, biosensors,[66] vaccines/immunotherapy,[67] among others.[68,69]

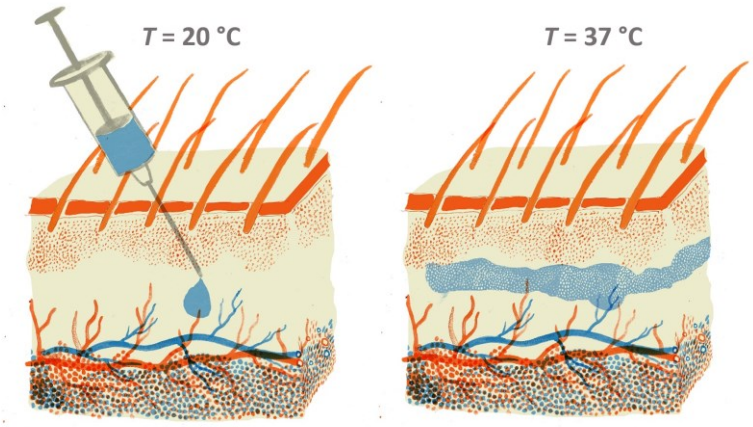

Figure 3. Scheme of injectable depot of thermoresponsive polymer: polymer dissolves in water at low temperature (left), but aggregates at body temperature upon administration (right);

adapted from literature and modified.[13]

1.4. Pharmacokinetics and pharmacodynamics of thermoresponsive polymers

Despite the great interest in medicinal research of thermoresponsive polymers, the knowledge of the actual polymer's fate and the pharmacokinetics of polymer's elimination is still very limited.[13,70,71] Data from one study indicate that the dissolution of the intramuscularly-administered poly(*N*-isopropylacrylamide), M_W = 28 kg/mol depot follows a two-phase kinetics: during the first phase the signal decreases quickly for a number of days, which is followed by a period of slow decrease over several weeks.[70] This study showed that the polymer is released from the body *via* urine and faeces nearly equally.[70] Another study regarding the biodistribution of the LCST-exhibiting polymers focused on the poly(*N*-(2,2-difluoroethyl)acrylamide):[13] the study has shown that the copolymers with various amounts of 2-hydroxyethyl acrylamide co-monomer (hydrophilic; non-ionic monomer; it does not exhibit thermoresponsive properties) in various ratios can alter both the phase-separation temperature of the aqueous solutions as well as the biological half-life of the polymer.[13] The study has also suggested a possible kinetics model.[13] Nevertheless, these models are limited to only a handful of (co)polymers, and a systemic study of pharmacokinetics of various thermoresponsive copolymers is still missing in the literature.

1.5. Polymer characterization

1.5.1. NMR spectroscopy

Nuclear magnetic resonance (NMR) is a useful spectroscopic technique that enables to determine the chemical formulas of compounds in a sample. This method can assess the concentration most nuclides and distinguish the atoms from different moieties (works for nuclides, where the spin quantum number, *S*,[i] is non-zero; such as ^{1}H, ^{13}C, ^{19}F, ^{31}P or ^{119}Sn), making it a particularly useful tool in organic, inorganic and polymer chemistry.[74]

When an atom with spin quantum number (*S*) is exposed to external magnetic field, its spin states cease to have equal energies and the nucleus spin-related energies will split into N energetic states (**Equation 1**).

$$N = 2S + 1 \quad (1)$$

Where N is the number of energy states and S is the spin quantum number of the nucleus.[i] Noteworthily, if the spin quantum number is equal to zero, the nucleus has only one energetic

[i] For example, $S = 0$ for ^{4}He or ^{16}O, S = ½ for ^{1}H, ^{13}C, ^{19}F or ^{31}P, $S = 1$ for ^{2}H, ^{17}O, and $S = 9$ for ^{180m1}Ta.[72,73]

state and therefore no energy split in the external magnetic field is observed. If the nucleus has only 2 possible states (for S = ½), the difference of energies between the two energetic states (ΔE) can be calculated with **Equation 2**:

$$\Delta E = -\gamma \hbar B \tag{2}$$

where γ is the gyromagnetic ratio of the nucleus; $\hbar$ is the reduced Planck's constant (also known as Dirac constant; ≈ $1.055 \cdot 10^{-34}$ J·s) and B is the magnetic field. As a result, these non-equal energy states will have different spin populations. The ratio of population high-energy spin (N_1) to low-energy spin state (N_0) follows Boltzmann distribution (**Equation 3**):

$$\frac{N_1}{N_0} = \boldsymbol{e}^{\frac{\gamma \hbar B}{k_B T}} \tag{3}$$

where $\boldsymbol{e}$ is the Euler's number (≈ 2.718) and k_B is the Boltzmann constant (≈ $1.381 \cdot 10^{-23}$ kg·m^2·s^{-2}·K^{-1}). Therefore, in the ground state, low-energy spin state is slightly more populated than the high-energy spin state. However, the state populations can be inverted with an electromagnetic pulse (excitation pulse) with a frequency close to that of Larmor frequency[ii] of the nucleus. Subsequently, these excited atoms gradually return into their ground state (the duration of this process is described by parameter T_1, which varies from a few microseconds to a few seconds).[72] However, until they return into their ground state, the excited nuclei undergo a nuclear precession, in which they induce temporary fluctuations of magnetic field, that can induce a current in nearby coils, thus generating a signal. These temporary fluctuations of magnetic field may be ascribed to Larmor precession; their frequency can be described with **Equation 4**:

$$\omega = -\gamma B \tag{4}$$

where ω is the angular frequency (Larmor frequency); γ is the gyromagnetic ratio of a nuclide (constant for specific nuclides[ii]) and B is the overall magnetic field effecting the nuclei. Nevertheless, the overall magnetic field (B) can be described as a difference of external magnetic field (B_0) and the magnetic field originating from the local electron movements (B_shiled) and local "shielding" (**Equation 5**).[72]

$$B = B_0 - B_\mathrm{shiled} \tag{5}$$

[ii] For example, the magnetic ratio is $267.52 \cdot 10^6$ rad·s^{-1}·T^{-1} for ^{1}H; $285.35 \cdot 10^6$ rad·s^{-1}·T^{-1} for ^{3}H; $67.28 \cdot 10^6$ rad·s^{-1}·T^{-1} for ^{13}C; $27.12 \cdot 10^6$ rad·s^{-1}·T^{-1} for ^{14}N; $-36.28 \cdot 10^6$ rad·s^{-1}·T^{-1} for ^{17}O; $251.81 \cdot 10^6$ rad·s^{-1}·T^{-1} for ^{19}F; $108.39 \cdot 10^6$ rad·s^{-1}·T^{-1} for ^{31}P; $8.68 \cdot 10^6$ rad·s^{-1}·T^{-1} for ^{56}Fe; $156.92 \cdot 10^6$ rad·s^{-1}·T^{-1} for ^{205}Tl.[72]

Therefore, each atom in the molecule exhibits slightly different Larmor frequency (ω) because it is exposed to a slightly different magnetic field. This difference of Larmor frequencies can be ascribed with a chemical shift factor (δ, **Equation 6**).[72]

$$\delta_{\text{sample}} = \frac{\omega_{\text{sample}} - \omega_{\text{ref}}}{\omega_{\text{ref}}} \quad (6)$$

where δ_{sample}[iii] is the chemical shift of the study atom, ω_{sample} is the Larmor frequency of the study atom and ω_{ref} is the Larmor frequency of a reference atom from a reference compound (determined by International Union of Pure and Applied Chemistry, IUPAC[iv]).[4,72,73,76] Because chemical shifts tend to be very low numbers, their values are usually expressed in parts per million (ppm).[iii]

The recorded signal as a function of time can be processed using Fourier transform to obtain NMR spectrum. Each peak corresponds to a specific atom or a moiety (they are characterized by their unique chemical shift), and the signal integral is linearly proportional to the concentration of this moiety in the sample.[73]

Furthermore, advanced NMR techniques can employ cross-polarisation (crossing of excitation from one atom to another), mixing and evolution of signal in time.[74] Most important advanced NMR techniques are attached proton test (APT) and distortionless enhancement by polarization transfer (DEPT) which can distinguish CH_3 moieties from CH_2 and CH in ^{1}H NMR spectrum, correlation spectroscopy (^{1}H-^{1}H COSY), which correlates the ^{1}H signals with *J*-coupling constant of ≈ 2 Hz or higher, and heteronuclear single-quantum correlation spectroscopy (^{1}H-^{13}C HSQC), which correlates ^{1}H and ^{13}C spectra and enables the assignment of hydrogens and carbons from one moiety.[74]

1.5.2. Size exclusion chromatography

Size-exclusion chromatography (SEC) is a chromatographic technique that enables the separation of molecules by their size. This method is very useful when working with a mixture of macromolecules (usually in biochemistry and in polymer chemistry).[77,78]

The stationary phase of SEC is a porous material with defined pore-size (such as Sephadex® G-25 or Sepharose® 2B). If sample contains both small and large molecules

[iii] The values of chemical shift are specific for the atom (regardless of isotope) and its chemical surrounding. For example, hydrogen atoms most commonly have chemical shift ranging from –1 to 12 ppm; fluorine atoms from –400 to 700 ppm; phosphorus atoms from –180 to 250 ppm, cobalt atoms from –4000 to 14000 ppm.[75]

[iv] For example, the reference compound for ^{1}H NMR and ^{13}C NMR is tetramethylsilane; for ^{19}F NMR is trichlorofluoromethane, for ^{31}P NMR is phosphoric acid and for ^{119}Sn NMR is tetramethylstannane.[73]

(salts, dyes) can interact with the pores and get adsorbed ("stuck") in them, while large molecules (polymers, proteins) cannot interact with these small pores due to steric hinderance. As a result, large molecules usually pass through the column rather quickly, while small molecules are delayed.[77,78] Furthermore, the retention factor of a polymer can be used to estimate the molar weight of the macromolecule.[78]

1.5.3. Turbidimetry

Turbidimetry is a spectroscopic technique that measures the decrease in transmitted light intensity caused by scattering or absorption.[42] Turbidimetry can determine the T_{CP} of a given system because the polymer aggregation (in most cases) increases the scattering rate of the sample. This method is widely available, quick, sensitive, and reasonably robust, accurately providing the T_{CP} at both low and relatively high concentrations.

Noteworthily, the beam wavelength,[8,42] heating and stirring rates,[42] and the selected threshold absorbance[8,42] may alter the measurement sensitivity and thus shift the experimental T_{CP}.[42] Furthermore, the increase of scattering rate during polymer aggregation depends on the dn/dc of the polymer solution.[42,44] If the dn/dc were equal to 0.00 mL·g^{-1} (rare, but possible), the polymer aggregation does not increase the turbidity of the sample, thus preventing from use of turbidimetry to determine the T_{CP}.[42,44]

1.5.4. Refractive index increment (dn/dc)

The refractive index increment (dn/dc) of a solution is a constant that describes the variation of the refractive index (n) with the solute concentration (c).[79] This constant depends on many parameters but mostly on the chemical structure of solute and solvent, sample density, pressure, temperature and wavelength of the light passing through the sample.[42,79]

Refractive index increment can be measured with many techniques, but possibly the most convenient is the differential refractometry (**Figure 4**). In this method, monochromatic light passes through two triangular-prism cells, that together form a rectangular cuboid. Each cell is filled with a different media – one cell (reference cell) contains a medium with a known refractive index (usually water, pure solvent, or saturated aqueous solution of KCl); the other cell contains a sample solution with an unknown refractive index. The difference of refractive indexes of media between sample and reference causes a shift of beam light, which can be detected using photodiodes. Because the magnitude of beam light shift is proportional to the difference of refractive indexes, the change of signal in photodiodes can be used to calculate the refractive index of sample. Lastly, the dn/dc can be determined from measurement of

refractive index of one sample in multiple dilutions; the refractive index increases/ decreases linearly with the solute concentration (if the solute concentration has only a negligible effect on the density of the solution).[80]

Knowing the value of systems' d*n*/d*c* is useful when determining T_{CP} turbidimetrically and it is critical for multi-angle light scattering (MALS) techniques to determine the concentration and the weight-average molar mass of polymers.[44,79] Furthermore, differential refractometers can be used as detectors in detection/characterization of polymers in size exclusion chromatography (SEC) and high-pressure liquid chromatography (HPLC).[81–83]

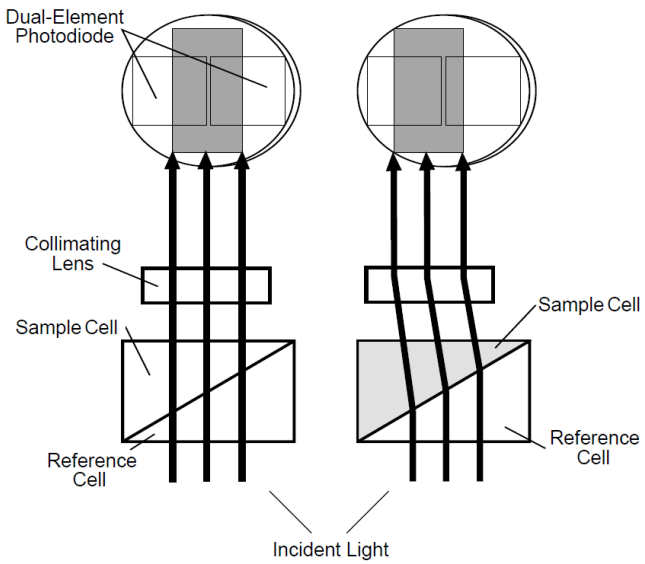

Figure 4. The principle of differential refractometry; figure adapted from literature[80] and modified.

1.5.5. Dynamic light scattering (DLS)

Dynamic light scattering is a physico-chemical technique that enables to determine the size distributions of particles in a suspension.[44] This method assesses the particle size distribution from the fluctuations of intensity of the transmitted light.[84]

The diffusion coefficient of a particle (D, $m^2 \cdot s^{-1}$) is affected by the hydrodynamic radius of the particle (R_h, m), which can be derived from Stokes-Einstein equation (**Equation 7**):

$$D = \frac{k_b T}{6\pi\eta R_h} \tag{7}$$

where k_b is Boltzmann constant ($1.381 \cdot 10^{-23}$ $kg \cdot m^2 \cdot s^{-2} \cdot K^{-1}$), T is the temperature (K), η is viscosity of the media ($kg \cdot m \cdot s^{-2}$).

The Brownian motion of particles in the sample solution can cause a fluctuation of transmittance of the sample (**Figure 5**). While the motion of small particles causes only a small decrease of intensity (because these particles obscure only a small area) for a short time (because their diffusion is fast), large particles cause a large decrease of intensity and for a longer time (because obscure a large area and their diffusion is slower than that in small particles).[44,84] Furthermore, the transmittance as a function of time can be measured from different angles simultaneously and the data from various angles can be correlated to obtain delay time (τ, s).[44,85]

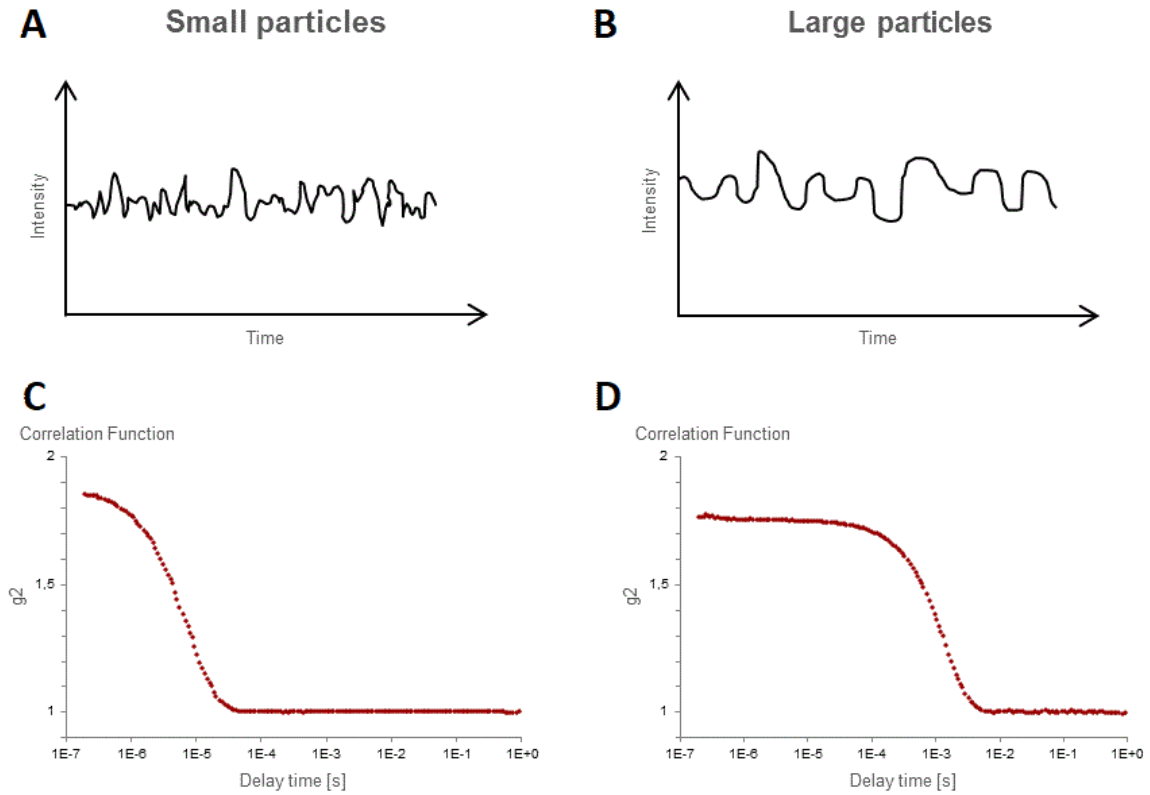

Figure 5: Comparison of fluctuations of beam intensity caused by Brownian motion of small (**A**) and large particles (**B**), and corresponding autocorrelation functions (**C**, **D**). The figure was adapted from literature[86] and modified.

The delay time (τ) provides the information about the size of the particle.[44] Therefore, upon complex processing,[87,88] the intensity as a function of time can provide the information about the size distribution of the particles in the sample. This information may be useful when assessing the T_{CP} of a polymer solution,[81,82] determining the critical association concentrations (CAC) of a compound,[59] and determining how CAC changes as a function of temperature or oxidation state.[59]

1.5.6. Isothermal titration calorimetry

Isothermal titration calorimetry (ITC) is a physico-chemical technique used to determine the thermodynamic parameters of interactions in solutions. This technique is commonly used in biochemistry and supramolecular chemistry to investigate the interactions between proteins, complexes, or ligands with receptors.[89,90]

Firstly, a solution of analyte is equilibrated to a target temperature in a thermally isolated reaction chamber. Subsequently, the system equilibrium is disrupted by (consecutively) adding small portions of titrant, while measuring the heat flux caused by the establishment of a new equilibrium (due to formation of new bonds between titrator and analyte). Then, this procedure is repeated, but analyte is replaced with pure solvent (blank experiment; titration of titrator into solvent). By subtracting the heat flux from blank experiment from the heat flux of the sample titration, we can obtain a complex titration isotherm,[90] which provides the information about the thermodynamics and stoichiometry of analyte-titrator interactions. This data is then fitted with a properly chosen model for the investigated complexation reaction (most commonly Wiseman isothermal model[90]), thus obtaining the information about the reaction enthalpy (ΔH, $\mathrm{J \cdot mol^{-1}}$), reaction entropy ($\Delta S$, $\mathrm{J \cdot mol^{-1} \cdot K^{-1}}$), multiplicity of binding sites (n), and many more.[90]

1.6. *In vitro* biological properties

1.6.1. *In vitro* cytotoxicity

In vitro cytotoxicity is a property of a compounds that describes their toxic effect on a given cell lines *in vitro*. Cytotoxicity is usually determined by studying the cell viability as a function of the study-compound concentration in the cultivation media. The assessment of cytotoxicity is highly desirable to prevent the administration of toxic drug-candidates into living organism.[91]

The most common cytotoxicity assay is the MTT (3-(4,5-dimethylthiazol-2-yl)-2,5-diphenyltetrazolium bromide) assay.[92] In this assay, the cells are incubated in an appropriate medium and temperature for a predetermined time. After the initial incubation, a sample of study compound or pure solvent (control experiment) is added to the cells and the cells are incubated for 24 or 48 hours.[92] Afterwards, MTT is added to the cells. MTT is a colourless-to-yellow compound, but it can be metabolised in the mitochondria of living cells into purple 1-(4,5-dimethylthiazol-2-yl)-3,5-diphenylformazan (formazan).[93] After a predetermined time, the concentration of formazan (linear to cell viability) is determined spectrophotometrically and compared to that in control cells. The results are usually expressed as a decrease of cell viability: if the viability decreases to 70% or lower of control group, the compound is considered cytotoxic.[91] Although the MTT assay is very convenient and used to be the standard test, recent

studies have shown that MTT can be reduced to formazan by ascorbate, cysteine, glutathione, among others, increasing the possibility of false negative cytotoxicity.[93] Furthermore, both MTT and formazan may accumulate in cellular lipidic structures and be oxidized/reduced without the presence of oxidoreductase enzymes.[93] As a result, the MTT is considered obsolete (but still accepted)[91] and is commonly replaced by other methods, such as resazurin assay.[91]

Resazurin assay (also known as alamarBlue™ or PrestoBlue™, among others) is a similar method to MTT assay that utilizes a different dye, resazurin (green fluorescence) which is oxidized to resorufin (orange fluorescence) in living cells.[94] The Alamar Blue assay appears to be more sensitive, specific and selective assay for determining the cellular cytotoxicity than the standard MTT assay.[91,95]

1.7. *In vivo* biological properties

1.7.1. Pharmacokinetics

The pharmacokinetics of a compound can be described by following phases: **l**iberation, **a**bsorption, **d**istribution, **m**etabolism, **e**xcretion (acronym **LADME**; liberation is often disregarded and acronym **ADME** is used instead).[96,97]

1) **Liberation.** After the administration of a drug in a specific drug-form, the drug formulation degrades and releases its drug content. The drug release can be intentionally designed to be as fast as possible (if the desired effect should occur quickly), or it can be intentionally prolonged to ensure a steady level of drug for management of chronic problems (usually in chronic/preventive treatment).[96,97]

   The liberation phase is relevant only to some routes of drug administrations, mostly in *per os*, but also in rectal, or vaginal routes of administration. Nevertheless, the liberation phase can be disregarded in intravascular route of administration.[96,97]

2) **Absorption.** The liberated drugs can be absorbed into the body and enter systemic circulation. The absorption of drugs can be passive through membranes (no transporter required for the uptake, *e.g.* oxygen or carbon dioxide); facilitated passive (heme-carrier protein 1 in heme absorption)[98] or active (requires specific transporters and energy, such as SGLT1, which actively transport glucose[99]).[96,97] The absorption phase can be disregarded in intravascular route of administration.[96,97]

3) **Distribution.** The absorbed drug is then carried through the bloodstream into the whole body, from which it can enter organs including the target organs.[96,97] However, the final concentration of drug in each organ does not necessarily have to be the identical. Very

lipophilic molecules may accumulate preferentially in adipose tissue (*e.g.* *N*-acetyldesipramine[100]); the biodistribution can be influenced by facilitated/active transport out of tissue (*e.g.* loperamide[101]) or into the tissue (*e.g.* 2-deoxy-2-[^{18}F]fluoroglucose into neurons or tumours;[102] choline derivatives into tumours[103]).[104]

4) **Metabolism.** The xenobiotics can be metabolised into their metabolites with a broad range of chemical reactions. Most commonly, the xenobiotics can be oxidized (this may involve cytochromes P450),[105] hydroxylated, reduced, epoxidized, hydrolysed or condensed with a large moiety to increase the compound's hydrophilicity to allow subsequent renal elimination (glucuronic acid, sulphuric acid, glycine).[96,97,106]

5) **Excretion.** Finally, the administered drug or its metabolites can be excreted from the target organ into the bloodstream and from there out of the body. The most common excretion ways include kidney (typical for highly hydrophilic molecules) and bile (typical for large and relatively hydrophobic molecules); other ways are rare, but possible (*e.g.* lungs for volatile compounds,[107,108] skin or milk).[96,97]

1.7.2. *In vivo* biodistribution

Biodistribution of the study compound (for example drugs, toxins, metabolites) is the description of its distribution throughout the organism as a function of time. The presence of a compounds in an organ may be a prerequisite to the desired biological effect, but its presence in other organs may cause undesired side effects. Therefore, knowing compounds' biodistribution in the organism may be crucial to its biomedical applications. The biodistribution of a compound can be determined in following ways:

1) **Administration of compounds and subsequent *ex vivo* determination**. The study compound is administered into the organism and the samples of tissues or body fluids are collected (for example blood, tissue, urine, faeces, saliva). The compounds of interest are extracted and subsequently separated, analysed, and quantified (for example by HPLC with UV-vis detector).[109] This analysis enables the evaluation of compound's concentration as a function of time within the given fluid/ body compartment. Although this method is direct and provides reliable results, the concentrations of compounds in the body fluids may be too low for UV-vis detection or mass spectroscopy. Furthermore, this direct method is difficult to use when the compound of interest can be metabolised: the metabolites may have a different HPLC-retention times from the original compounds making it harder to track them.[109]

2) **Administration of compounds labelled with radioisotope**. The presence of radioisotope can significantly improve the sensitivity of compounds detection, thus enabling us to work with lower concentrations of compounds. Furthermore, this method enables the detection of metabolites of the administered compounds (if the radiolabelled moiety is not cleaved during the metabolism). However, working with radioisotopes has its disadvantages: it required skilled personnel, radionuclides are costly, and the labelled compounds decay quickly while exposing patients/ lab animals and personnel to radiation. This method can be used *in vivo* or *ex vivo*:

   a) ***Ex vivo* biodistribution.** In this method, samples of tissue/ body fluids are collected at various timepoints, and the concentration of radioisotope is assessed. The presence of radioisotope can be utilized to increase the sensitivity and specificity of the measurement. Body fluids are collected, the compounds of interest are separated, analysed, and quantified (for example by HPLC with a radio-detector). A great advantage of this method is, that it enables the determination (and possibly isolation) of drug-metabolites.[110,111]

   b) **Single Photon Emission Computer Tomography (SPECT)** is a tomographic imaging technique that enables the detection of radioisotope biodistribution *in vivo*. The study compound is traced with radioisotope, commonly ^{67}Ga ($t_{½}$ = 67 h, E = 1.0 MeV), ^{99m}Tc ($t_{½}$ = 6.0 h, E = 140 keV), ^{111}In ($t_{½}$ = 2.8 d, E = 860 keV), ^{123}I ($t_{½}$ = 13.2 h, E = 159 keV) or ^{131}I ($t_{½}$ = 8.0 d, E = 971 keV).[112,113] SPECT is commonly used in clinical practice to asses the biodistribution of tracers with known affinity towards some tissues/ pathologies, such as ^{99m}Tc-sestamibi (for myocardial perfusion imaging[114]) or ^{99m}Tc-exametazime (for functional brain imaging[115]), among others.[112]

   c) **Positron Emission Tomography (PET)** is a tomographic imaging technique that enables the detection biodistribution of a radioisotope. The study compound is traced with radioisotope, commonly ^{11}C ($t_{½}$ = 20 min, E = 1.98 MeV), ^{13}N ($t_{½}$ = 10 min, E = 2.22 keV), ^{18}F ($t_{½}$ = 110 min, E = 1.66 MeV), ^{68}Ga ($t_{½}$ = 68 h, E = 2.92 MeV), ^{64}Cu ($t_{½}$ = 12.8 h, E = 1.68/0.58 MeV), or ^{124}I ($t_{½}$ = 4.2 d, E = 3.16 MeV).[112,113] PET is commonly used in clinical practice to asses the biodistribution of tracers with known affinity towards some tissues/ pathologies, such as 2-deoxy-2-[^{18}F]fluoroglucose (for tumour and neurological imaging[102]) or choline derivatives (for tumour imaging[103]), among others.[112] Although PET imaging hardware is more demanding and expensive than SPECT hardware, the resulting image of PET can have a significantly higher resolution

and contrast than that of SPECT. As a result, PET imaging is becoming more and more common in the clinics.

3) **Administration of compounds labelled with MRI tracer/ contrast agent.** Magnetic resonance imaging (MRI) is a clinically used diagnostic tool, which posses as an alternative to radioactive tracing. This method uses gradients of magnetic fields and high-frequency pulses to assess the presence of nuclides. The nuclides with high gyroscopic ratios (such as ^{3}H, ^{19}F, ^{3}He, ^{205}Tl, ^{203}Tl, or ^{35}P see **Figure 6**)[72] are advantageous for heteronuclear MRI (because they have a high sensitivity).[13,59,116] Furthermore, it is highly desirable if the nuclide is commonly available and no isotope enrichment is required. Of all elements, monoisotopic ^{19}F is the most prominent element for heteronuclear MRI.[116] Although, heteronuclear MRI has relatively low sensitivity, it is a promising alternative to PET and SPECT that does not involve any radioisotopes.[116]

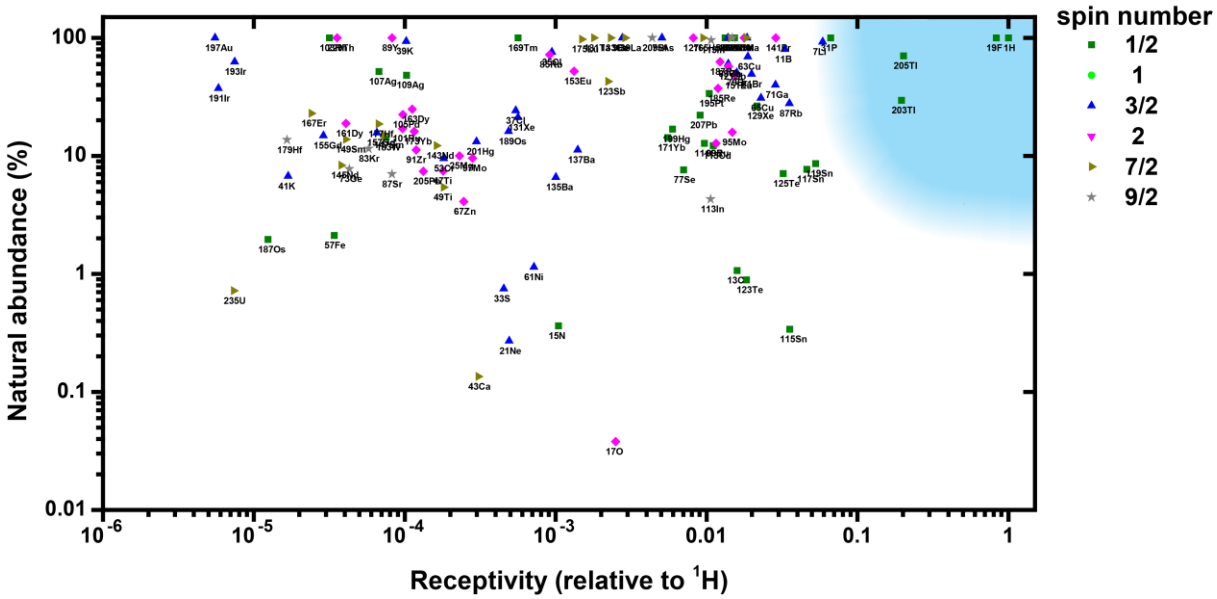

Figure 6. Natural abundance of the selected nuclides and their receptivity relative to ^{1}H,[v] based on data in the literature.[72] The blue area shows the most suitable nuclides for heteronuclear MRI.

Additionally, the compounds can be traced with a moiety that alters the MR relaxation properties of the surrounding water and thus increases the signal of ^{1}H MRI (usually chelates of lanthanides).[117] Although this is rather an elegant method with reasonably high sensitivity,

[v] Receptivity, also called sensitivity, is a quantity that, in layman's terms, describes how "easily" the nucleus can be detected. Its value is equal to $\gamma^3 \cdot I \cdot (I + 1)$

the lanthanide chelates are large to very large moieties that can alter the biodistribution of the molecule.

4) ***In vivo*** **fluorescence imaging** is a non-invasive imaging technique that enables the localization of fluorescent compounds in living organisms. In this method, strong light with a wavelength corresponding to the excitation wavelength of the fluorescent compound irradiates the organism and excites the fluorescent compound. Subsequently, the excited dye return into its ground state and emits light corresponding to its emission wavelength. Lastly, the light emissions can be used to track the location and concentration of fluorescent compound.

This method is rather elegant but has many limitations preventing its massive use (especially in human medicine). The light penetration through the skin is limited (**Figure 7**); therefore, this method is suitable for imaging of subcutaneous compounds in small animals (especially when their skin is thinner). Furthermore, the signal depends heavily on the geometry of the subcutaneous depots and its depth. The lowest extinction coefficients are in red-to-infrared region;[118] therefore, ideally both excitation and emission wavelengths should be in this region.

Despite these disadvantages, the *in vivo* fluorescence has numerous advantages: with properly chosen fluorescence dyes, its sensitivity is high; nor the imaging, neither the dyes damage the surrounding tissues (unlike radioisotopes), and the technique is safe for the personnel and requires relatively little safety precautions (unlike radioisotopes). The method is suitable for observing the dissolution of subcutaneous depots of fluorescent compounds because the geometry of the depot changes only negligibly as a function of time and most changes can be ascribed to the decrease of dye concentrations.

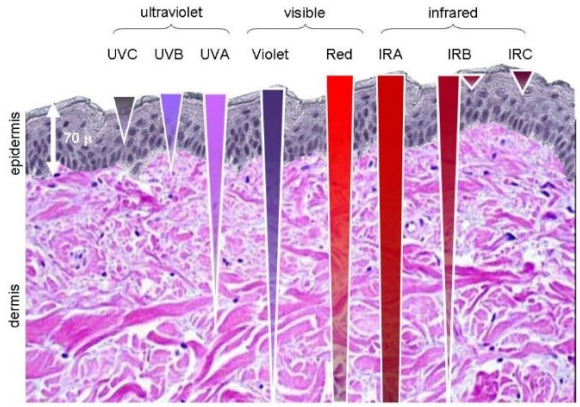

Wavelength of light (nm)	Light	Penetration depth (mm)
250-280	UV-A	0.04
300	UV-B	0.10
360	UV-C	0.19
400	violet	0.25
700	red	0.40
1200	IR-A	0.80
2000	IR-B	0.40

Figure 7. Light penetration in the human skin. Penetration depth is defined as a depth, where the light is attenuated down to 1%. Adapted from literature[118] and modified.

2. Aims of the Thesis

The aim of this thesis is to synthesize and characterize thermoresponsive polymers and determine the pharmacokinetics of their intramuscularly administered depot.

1) Poly[(*N*-2,2-difluoroethyl)acrylamide], poly[(*N*-isopropyl)acrylamide], poly[(*N*,*N*-diethyl)acrylamide], and poly[(*N*-acryloyl)pyrrolidine] will be prepared by RAFT polymerization in three different molar weights each (≈ 20 to 25, 30 to 35, and 40 to 50 kg/mol, **Figure 8**).
2) The RAFT reagent will be removed and replaces with inert moiety. The resulting polymers will be characterized using SEC and NMR.
3) The study polymers will be thoroughly characterized in different biologically relevant media (water, PBS, FBS) using turbidimetry, DLS, and calorimetry. The effect of ions on the T_{CP} will be described.
4) The polymers will be labelled with fluorescent dye (Cy7-amine).
5) The polymer purity and chemical stability of the fluorescent label will be determined using GPC.
6) The cytotoxicity of the study polymers in relevant cell lines will be determined.
7) The fluorescent dye-labelled polymers will be administered into mice and the polymer biodistribution (signal as a function of time) will be determined using fluorescence imaging.
8) The obtained data from biodistribution will be used to suggest a biodistribution model of polymer.
9) A histological examination of mice will be performed to investigate any possible long-term side effects of polymer administration.
10) All data will be evaluated. A correlation between physico-chemical properties of the polymers and its biological retention will be investigated.

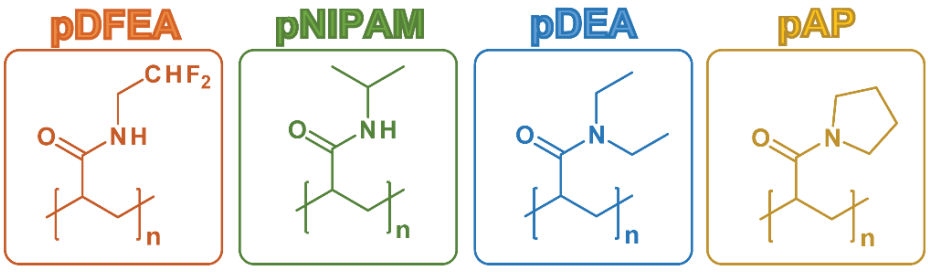

Figure 8. Structures of the study polymers: poly[(*N*-2,2-difluoroethyl)acrylamide] (**pDFEA**), poly[(*N*-isopropyl)acrylamide] (**pNIPAM**), poly[(*N*,*N*-diethyl)acrylamide] (**pDEA**), and poly[(*N*-acryloyl)pyrrolidine] (**pAP**).

3. Experimental Section

3.1. Materials

N,N-dimethylformamide (DMF), methanol (MeOH) and diethyl ether were purchased from Lach-Ner s.r.o. (Neratovice, Czech Republic) in analytical quality. DMF was dried with 3.0 Å molecular sieves for at least 7 days. MeOH-4d (99.80% D) was purchased from Eurisotope (Saint-Aubin, France). 2,2-Difluoroethylamine was purchased from Fluorochem (Derbyshire, UK). Argon 5.0 ($c_{Ar} \geq 99.999\%$) was purchased from Messer Technogas s.r.o. (Prague, Czech Republic). Foetal bovine serum (FBS, qualified, heat inactivated, 10500-064, LOT 2165873H) was purchased from Thermo Fisher Scientific (Waltham, MA, USA). Cy7-amine was purchased from Lumiprobe (Hannover, Germany). Sephadex™ LH-20 was purchased from GE Healthcare (Chicago, MI, USA). Resazurin (PrestoBlue™) dye was purchased from Thermo Fisher Scientific (Waltham, MA, United States); penicillin and streptomycin were purchased from Thermo Fisher Scientific (Waltham, MA, USA). The remaining chemicals were purchased from Sigma-Aldrich s.r.o. (Prague, Czech Republic).

Foetal bovine serum, and Cy7-amine were stored at –22 °C; monomers, their precursors, NMR solvents were stored at 4 °C; the remaining chemicals were stored in a dry, dark storage at ambient temperature. All chemicals were used without any additional purification, unless stated otherwise. Human Fibroblast (HF) kindly provide by IEM AV ČR (Institute of experimental medicine) and rMSC (rat mesenchymal stem cell) from IKEM (Institute of clinical and experimental medicine).

The mice feed (Altromin 1324 Velaz - maintenance diet) was obtained from Velaz, s.r.o. (Prague, Czech Republic). Visidic® 2 mg/mL gel (Bausch+Lomb, Laval, Canada) was used for eye protection of the mice during anaesthesia. Isoflurane for anaesthesia of the experimental animals was purchased (AErrane 100 %) from Baxter Healthcare Ltd. (Norfolk, UK). We used H&E Fast Staining Kit Art. No. 9194 and Van Gieson Trichrome Staining Kit 9193.1 stains for histological examinations (Carl Roth GmbH + Co. KG, Karlsruhe, Germany); the corn oil was purchased from Sigma-Aldrich s.r.o. (Prague, Czech Republic).

3.2. Instruments and used methods in polymer synthesis and characterizations

3.2.1. NMR spectroscopy

All NMR spectra were measured on a Bruker Avance III HD 400 MHz spectrometer (Bruker, Billerica, MA, USA) equipped with a broadband probe. All compounds (5 to 10 mg) were dissolved in MeOH-4d (0.50 to 0.80 mL). The following spectra were assessed: ^{1}H NMR (32 scans, relaxation delay 30.0 s), ^{13}C NMR (^{1}H decoupled, 1024 scans, relaxation delay

2.00 s), ^{19}F NMR (64 scans, relaxation delay 5.00 s), ^{1}H-^{13}C multiplicity-edited HSQC (heteronuclear single quantum coherence spectroscopy)[119,120] (2 scans, relaxation delay 1.50 s, size of the fid 2048 by 256, spectral width 14.0 by 200 ppm, using ^{1}H and ^{13}C external projections), see **Figure S1-S20**. These spectra were used to confirm the polymer structure and to determine the purity; the multiplicity-edited HSQC spectra (**Figure S3**, **S7**, **S11**, **S14**, **S17** and **S20**) were used for peak-matching. The spectra were processed in TopSpin 3.6.1 (Bruker, Billerica, MA, USA) and MestReNova 6.0.2 (Mestrelab Research S.L., Santiago de Compostela, Spain), trace contaminates were assigned according to reference.[121]

3.2.2. Size exclusion chromatography (SEC)

The number-average molar mass (M_n), weight-average molar mass (M_w), and polymer dispersity ($Đ_M = M_w/M_n$) were determined by SEC using an HPLC Ultimate 3000 system (Dionex, Sunnyvale, CA, USA) equipped with an SEC column (TSKgel SuperAW3000 150 × 6 mm, 4 µm). Three detectors, UV/VIS, refractive index (RI) Optilab®-rEX and multiangle light scattering (MALS) DAWN® EOS (Wyatt Technology Co., Santa Barbara, CA, USA), were employed with a methanol (A) and sodium acetate buffer (B, 0.3 M, pH 6.5) mixture (A:B = 80:20 v/v, flow rate of 0.6 mL·min^{-1}) as the mobile phase (**Figure S21-S24**). The dn/dc the for the given mobile phase and polymers was 0.1100 (**pDFEA**), 0.1540 (**pNIPAM**), 0.2015 (**pDEA**), and 0.1646 mL·g^{-1} (**pAP**) at wavelength 620 nm and 20 °C.

3.2.3. Turbidimetry

Turbidimetry was measured with Crystal16™ parallel crystalliser turbidimeter (Avantium Technologies, Ontario, Canada) connected to a recirculation chiller and dry compressed air. Aqueous polymer solutions were heated from 10.0 °C to 55.0 °C (in some cases to 80.0 °C) with a heating rate of 0.5 K·min^{-1}, followed by cooling to 10 °C and maintaining this temperature for 30 min. Each measurement was repeated 6 times; the samples were stirred at 700 rpm.

All polymers were dissolved in ultrapure water, phosphate buffered saline (PBS, 140 mM, pH = 7.40, Dulbecco type[122]) or foetal bovine serum (FBS) at a concentration of 1.25, 2.50, 5.00, 10.00, 20.00 and 40.00 mg/mL. The samples were stored at 4 °C prior to their measurement. Transmittance was monitored at λ = 600 nm, a sudden decrease of transmittance below 50% indicated the cloud point temperature.[42]

3.2.4. Refractive index increment (d*n*/d*c*)

We measured the refractive index increment (d*n*/d*c*) of all study polymers (in PBS in five different concentrations (*ca.* ≈ 0.12 to ≈ 2.3 mg/mL) using PSS DnDc-2010/620 differential refractometer (Polymer Standard Service, Mainz, Germany) at 620 nm and 29.0 °C. The data were processed using Differential Refractometer Software (version 5.32, Brookhaven Instruments Corp., Holtsville, NY, USA), see **Figure S54** to **S65**.

3.2.5. Dynamic light scattering (DLS)

We determined the size of the polymer assemblies using dynamic light scattering (DLS) by Zetasizer Nano-ZS, Model ZEN3600 (Malvern Instruments, Malvern, UK) at θ = 173° scattering angle and at 15.0 to 60.0 °C with a step of 0.5 °C and temperature equilibration for 2.0 min per step. The measurement was repeated 3 times at each step. All samples were filtered using 0.45 μm PVDF filters before the measurements. The data were evaluated using the Zetasizer software (Nano, version 7.10, Malvern, UK), JMalgen (v.2.0, Institute of Macromolecular Chemistry, Prague, Czech Republic), Genr (v.11, Institute of Macromolecular Chemistry, Prague, Czech Republic)[123] and MatLab (v.9.9.0.1467703, R2020b, The MathWorks, Inc., Natick, MA, USA). We present the DLS results as intensity-based size distributions because they entail smaller calculation errors than volume or number-based size distributions. However, larger particles scatter at a significantly higher intensity than smaller particles. Consequently, the results are biased towards the largest species in solution.[44]

3.2.6. Isothermal titration calorimetry

The solutions of polymers (**F3**, **I3**, **E3** or **P3**; each 10 mg/mL, 201 μL) in ultrapure water were titrated with PBS or FBS using ITC 200 titration calorimeter (Malvern Panalytical, Malvern, UK). In each run, 40 μL of PBS or FBS were added in consecutive injections (the first injection was always 0.1 μL; then with increment 0.5 or 1.0 μL). All samples were stirred at 1000 rpm and titrated at three temperatures: (i) below T_{CP}, 293 K for all polymers in all media; (ii) below T_{CP} in ultrapure water, but above T_{CP} in PBS or FBS, 301 K (**E3** and **F3**), 303 K (**I3**) and 323 K (**P3**); and (iii) above T_{CP} in all media, 313 K (**E3** and **I3**), 323 K (**F3**) and 333 K (**P3**). Subsequently, PBS and FBS were titrated to ultrapure water at all experimental temperatures to determine their heat of dilution (as blanks samples). Additionally, PBS and FBS were titrated (10×1 μL injections) to the solution of benzoic acid (0.25 mM ≈ concentrations of polymers) at 293, 313 and 333 K to estimate the thermal contribution of the neutralization reaction of terminal carboxylic group (see **Figure S41** in ESI for details).

The isotherms of complex shape were fitted with two independent binding sites model (using Wiseman model[90]), the ionic strength of PBS (162.7 mM) was accepted as a titrant concentration for both PBS and FBS. From the fit the reaction enthalpy change ΔH for the first binding site (kJ/mol of polymer) was extracted and normalized to concentration of monomeric units. Other fitting parameters (stoichiometry n and association constant K, M^{-1}) were not used in the discussion (see ESI, **Figures S37** to **S40** for details).

3.2.7. Data processing

All data were processed in Microsoft Office 365 Pro Plus 16.0 (Microsoft, Redmond, WA, USA) and OriginPro 8.6.0 (OriginLab Corporation, Northampton, MA, USA) unless stated otherwise. The schemes and structures were drawn in ChemDraw Professional 16.0.1.4 (77) (Perkin Elmer Informatics, Inc., Waltham, MA, USA). The graphics were processed in Adobe Illustrator CS6 16.0.0 (Adobe Systems Inc., San Jose, CA, USA).

3.3. Synthesis, purification, and characterization

3.3.1. Synthesis, purification, and characterization of monomers

The (*N*-acryloyl)pyrrolidine and *N*-(2,2-difluoroethyl)acrylamide were synthesized from acryloyl chloride and the corresponding amines (**Figure 9**) using a modified procedure inspired by literature;[5,124] the remaining monomers were purchased.

Pyrrolidine (18.7 mL, 16.2 g, 228 mmol) or 2,2-difluoroethylamine (14.0 mL, 16.8 g, 207 mmol), respectively, were mixed with triethylamine (34.0 mL, 24.8 g, 245 mmol), dissolved in dry tetrahydrofuran (THF, 250 mL), and cooled down to 0 °C on a water/ice bath. Acryloyl chloride (freshly distilled at atmospheric pressure, 20.0 mL, 22.4 g, 247 mmol) was dissolved in dry THF (40 mL), and this solution was added dropwise to the amine solution under constant stirring until cooling to 0 °C. After this step, the reaction mixture was stirred at room temperature for 7 hours and subsequently diluted with diethyl ether (500 mL) and filtered. The filtrate was washed with an aqueous $NaHCO_3$ solution, water, and saline using a separatory funnel. The organic phases were dried with $MgSO_4$, the solvent was removed using a rotary evaporator, and the product was purified by flash chromatography in multiple batches (mobile phase: ethyl acetate/hexane 1:2). The yields were 20.2 g (71%) for (*N*-acryloyl)pyrrolidine and 20.4 g (73%) for *N*-(2,2-difluoroethyl)acrylamide.

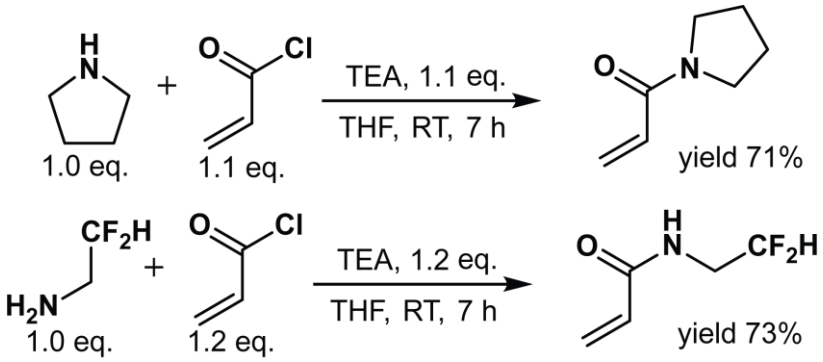

Figure 9. Synthesis of (*N*-acryloyl)pyrrolidine and *N*-(2,2-difluoroethyl)acrylamide from acryloyl chloride and the corresponding amines.

***N*-acryloylpyrrolidine**: ^{1}H (MeOH-4d): 6.62 (dd, J = 16.8, 10.4 Hz, 1H), 6.27 (dd, J = 16.8, 2.0 Hz, 1H), 5.74 (dd, J = 10.4, 2.0 Hz, 1H), 3.62 (t, J = 6.8 Hz, 1H), 3.50 (t, J = 6.9 Hz, 1H), 2.07-1.85 (m, 4H). ^{13}C: 165.1, 128.7, 126.6, 46.5, 45.7, 25.6, 23.8 ppm. (**Figure S1** to **S3**)

***N*-(2,2-difluoroethyl)acrylamide**: ^{1}H (DMSO-6d): 8.48 (t, J = 4.9 Hz, 1H), 6.28 (dd, J = 17.1, 10.1 Hz, 1H), 6.14 (dd, J = 17.1, 2.2 Hz, 1H), 6.04 (tt, J = 55.8, 3.8 Hz, 1H), 5.65 (dd, J = 10.1, 2.2 Hz, 1H), 3.57 ppm (tdd, J = 16.1, 6.0, 3.9 Hz, 2H). ^{13}C: 165.66, 131.40, 126.67, 114.95 (t, J = 239.7 Hz), 41.29 ppm (t, J = 25.6 Hz). ^{19}F: –121.79 ppm (dt, J = 55.9, 16.1 Hz). (**Figure S4** to **S7**)

3.3.2. Synthesis, purification, and characterization of polymers

Poly[*N*-(2,2-difluoroethyl)acrylamide] (**pDFEA**), poly(*N*-isopropylacrylamide) (**pNIPAM**), poly(*N*-diethylacrylamide) (**pDEA**) and poly(*N*-acryloylpyrrolidine) (**pAP**) were prepared by reversible addition−fragmentation chain-transfer polymerization (RAFT)[124] with 4-cyano-4-[(dodecylsulfanylthiocarbonyl)sulfanyl]pentanoic acid as the RAFT polymerization chain transfer agent (CTA)[76] and 4,4′-azobis(4-cyanovaleric acid) (ACVA) as the initiator (**Figure 10**).[124]

The polymerization mixture consisted of a specific monomer (1.50 to 2.00 g), CTA and ACVA in various molar ratios and dried DMF (**Table 1**). The mixture was bubbled with argon in an oven-dried Schlenk flask, heated to 70 °C in an oil bath and stirred with a magnetic stirring bar overnight. Subsequently, the product was precipitated in diethyl ether, filtered, and the polymer was re-dissolved in methanol and purified using a Sephadex™ LH-20 column and methanol as the eluent. The polymer-containing fractions were evaporated in a rotatory evaporator under reduced pressure, and the polymer was re-dissolved in water and isolated by freeze-drying.

Table 1. Volumes/ mass/ molar amount of solvent (V_{DMF}), monomers (m_{mon}, n_{mon}), charge transfer agent (m_{CTA}, n_{CTA}) and initiator (m_{ini}, n_{ini}) used in polymer synthesis

Polymer/code		V_{DMF} (mL)	m_{mon} (g)	n_{mon} (mmol)	m_{CTA} (mg)	n_{CTA} (µmol)	m_{ini} (mg)	n_{ini} (µmol)
	F1				21.2	52.5	4.41	15.8
pDFEA	**F2**	4.00	1.50	11.1	14.1	35.0	2.94	10.5
	F3				8.5	21.0	1.77	6.3
	I1				56.5	140	11.8	42.0
pNIPAM	**I2**	6.00	2.00	17.7	28.3	70.0	5.89	21.0
	I3				18.8	46.7	3.92	14.0
	E1				28.3	70.0	5.89	21.0
pDEA	**E2**	6.00	2.00	15.7	14.1	35.0	2.94	10.5
	E3				11.3	28.0	2.35	8.4
	P1				42.4	105	8.82	31.5
pAP	**P2**	4.00	1.50	12.0	21.2	52.5	4.41	15.8
	P3				14.1	35.0	2.94	10.5

After polymerization, the CTA group was removed by aminolysis using propylamine ($PrNH_2$), followed by nucleophilic addition of methyl acrylate to the thiol end-group in dry DMF under an argon atmosphere, as previously reported (**Figure 10**).[125] Polymer-CTA, propylamine, and tris(2-carboxyethyl)phosphine hydrochloride (to prevent the oxidation of thiols to disulphides[126]) were dissolved in DMF (5.00 mL). The reaction mixture was stirred for 120 min at room temperature under a nitrogen atmosphere. Methyl acrylate was added to the reaction mixture and stirred at room temperature for 24 hours. The polymers were purified using the procedure mentioned above. Yields are summarised in **Table 5**, amounts of reactant are summarized in **Tables 1** and **2**.

pDFEA: ^{1}H (MeOH-4d): 8.00 (1H), 5.95 (t, J = 56.1, 1H), 3.58 (t, J = 14.4 Hz, 2H), 2.18 (1H), 1.67 ppm (2H); ^{13}C: 176.2, 114.2 (J = 239.5 Hz), 41.8 (t, J = 28.1 Hz), 35.1 ppm; ^{19}F: –123.8 ppm (2F). (**Figure S8** to **S11**)

pNIPAM: ^{1}H (MeOH-4d): 7.63 (1H), 3.98 (1H), 2.11 (1H), 1.60 (2H), 1.17 ppm (6H); ^{13}C: 174.8, 42.9, 41.1-41.9, 35.0, 21.4 ppm. (**Figure S12** to **S14**)

pDEA: ^{1}H (MeOH-4d): 3.52-3.36 (4H), 2.65 (1H), 1.74-1.81 (2H), 1.13 ppm (6H); ^{13}C: 174.2, 40.2-41.8, 36.6, 36.1, 12.0-13.8 ppm. (**Figure S15** to **S17**)

pAP: ^{1}H (MeOH-4d): 3.1-3.8 (4H), 2.3-2.7 (1H), 1.96 (4H), 1.68 ppm (2H); ^{13}C: 173.7, 45.9-46.5, 39.0, 35.0, 24.0-25.7 ppm. (**Figure S18** to **S20**)

Table 2. Mass and molar amount of polymers (m_{pol}, n_{pol}), propylamine (V_{PA}, n_{PA}), tris(2-carboxyethyl)phosphine hydrochloride (m_{TCEP}, n_{TCEP}), and methyl acrylate (V_{MA}, n_{MA})

Polymer/code		m_{pol} (g)	n_{pol} (µmol)	n_{PA} (mmol)	V_{PA} (µL)	n_{TCEP} (µmol)	m_{TCEP} (mg)	n_{MA} (mmol)	V_{MA} (mL)
pDFEA	**F1**	1.00	38.2	1.91	81.2	38.2	11.0	6.69	550
	F2		27.6	1.38	58.7	27.6	7.9	4.83	400
	F3		20.2	1.01	42.9	20.2	5.8	3.54	290
pNIPAM	**I1**	1.00	49.5	2.48	105.2	49.5	14.1	8.66	710
	I2		31.6	1.58	67.2	31.6	9.1	5.53	450
	I3		20.6	1.03	43.8	20.6	5.9	3.61	290
pDEA	**E1**	1.00	44.8	2.24	95.2	44.8	12.8	7.84	640
	E2		28.8	1.44	61.2	28.8	8.3	5.04	410
	E3		24.2	1.21	51.4	24.2	6.9	4.24	350
pAP	**P1**	1.00	51.0	2.55	108.4	51.0	14.6	8.93	730
	P2		27.8	1.39	59.1	27.8	8.0	4.87	400
	P3		19.5	0.98	41.4	19.5	5.6	3.41	280

3.3.3. Polymer modifications (labelling with fluorescent dye)

We dissolved the polymers (100 mg each) in dry toluene (15 mL, 0.1-1.5 mL of acetone was added if needed) and evaporated the solvent using rotatory evaporator. This process was repeated five times, afterwards the polymers were maintained in vacuum ($p \leq 10$ mBar) at room temperature for 3 days to remove trace solvents. Subsequently, these polymers were traced with fluorescent dye (Cy7-amine, **Figure 16**) under various reaction conditions (**Table 3**) dry DMF under an argon atmosphere. The reaction was performed in a 2 mL reaction vessel for 14 hours at room temperature. Afterwards, DMF was evaporated using rotatory evaporator; the polymer was dissolved in methanol (0.5-1.2 mL) and purified by gel separation a using flash chromatography (puriFlash®, Interchim, Montluçon, France) with Sephadex™ LH-20 column using methanol as the eluent. The polymer-containing fractions were evaporated using rotatory evaporator; the polymer was dissolved in water the water was removed by freeze-drying (≈ –190 °C, ≈ 16.5 Pa, 20 hours). The temperature of the sample never exceeded 40 °C during the reaction, processing, or storage. The labelled polymers were stored in dark at –20 °C until their use.

Table 3. Masses and volumes of reactants in labelling of polymers with Cy-7 amine dye. The polymers (m_{pol}, n_{pol}) were dissolved in (V_{DMF}).

Polymer		m_{pol} (mg)	n_{pol} (μmol)	V_{DMF} (μL)	m_{Cy7} (mg)	n_{Cy7} (μmol)	m_{PyBOP} (mg)	n_{PyBOP} (μmol)	m_{DIPEA} (μg)	n_{DIPEA} (μmol)
pDFEA	**F1**	20.0	1.02	500	0.89	1.24	6.47	12.4	268	2.07
	F2	20.0	0.65	500	0.62	0.85	4.46	8.57	184	1.42
pNIPAM	**I1**	20.0	0.83	500	1.10	1.53	7.97	15.3	330	2.55
	I2	20.0	0.57	500	0.70	0.97	5.08	9.76	210	1.62
pDEA	**E1**	20.0	0.95	500	1.02	1.42	7.38	14.2	306	2.37
	E2	20.0	0.63	500	0.68	0.94	4.91	9.44	204	1.58
pAP	**P1**	20.0	1.14	500	1.23	1.70	8.87	17.0	367	2.84
	P2	20.0	0.61	500	0.66	0.91	4.75	9.13	197	1.57

3.3.4. Determination of dye concentration and polymer purity

The polymers were dissolved in a mixture of sodium acetate buffer (0.3 M, pH 6.5) and methanol (80:20 v/v; c_{pol} = 1.0 mg/mL). The mixture was stored at room temperature in dark and its composition was analysed within 1 hour, 50 hours and 200 hours after the preparation. The polymer purity was studied using SEC. The resulting spectra can be seen in **Figure S68**.

The d*n*/d*c* for the given mobile phase and polymers was 0.110 (**pDFEA**), 0.1540 (**pNIPAM**), 0.2015 (**pDEA**), and 0.1646 (**pAP**).

The polymer dye (Cy7-amine) concentration was determined *via* spectrophotometry (Sunrise microplate reader; Tecan Group Ltd., Switzerland) with an external calibration (**Figure S67** and **S68**) and the molar extinction coefficient of Cy7-amine was determined.

3.4. *In vitro* biological experiments

The cells (human fibroblasts, HF, and rat mesenchymal stem cells, rMSC) were cultivated in Dulbecco modified Eagle medium (DMEM) at 37 °C in 5% CO_2, with the phenol red indicator and supplemented with a heat inactivated 10% foetal bovine serum (FBS), penicillin and streptomycin. The adhered cells were incubated overnight in 25 cm^3 flask at 37°C in 5% CO_2 atmosphere before treatment.

The cells (HF or rMSC, respectively) were seeded in a 96-well plate (TPP, biotech) in the density $7 \cdot 10^3$ cells per well. Subsequently, thermosensitive polymers **F2**, **I2**, **E2**, or **P2** were dissolved in PBS at concentration from 0 to 100 μg/ml at room temperature and the solutions

were added to the cells. Afterwards, the cells were incubated for additional 72 hours, and the cell viability was assessed using resazurin assay (PrestoBlue™, ThermoFisher) according to manufacturer's instructions. Untreated cells (no added polymer; only pure PBS) were used as negative control; cells treated with 4 mM H_2O_2 in PBS were used as a positive control. The results were expressed as the viability percentage relative to negative control; the results were processed in GraphPad Prism5 software (GraphPad software, San Diego, CA, USA) using one-way analysis of variance (ANOVA) with the levels of significance $p \leq 0.05$.

3.5. *In vivo* biological experiments

The experiments described in this study were performed in the accordance with Act No. 359/2012 Sb. on the Protection of Animals Against Cruelty and Precepts 419/2012 Sb. and 299/2014 Sb. Ministry of Agriculture on the Protection of Experimental Animals (including relevant EU regulations as of 2020/2021). All mice experiments were conducted by authorized and experienced personnel according to the recommended laboratory practise guidelines.

3.5.1. General preparation

We performed all *in vivo* experiments using BALB/c strain female mice (6 weeks old, purchased from AnLab s.r.o, Prague, Czech Republic). The mice were housed according to the approved guidelines (in individually ventilated cages with the sterilised bedding and cellulose sheets, 12:12 hours light-dark cycle at 22 ± 1 °C and 60 ± 5% humidity), their feed Altromin 1324 Velaz (maintenance diet) and water (purified by Smart N-II, Heal Force Bio-meditech Holdings Limited, Shanghai, China) were provided *ad libitum*. The BALB/c mice ($n = 42$) were let to acclimatize for 5 to 7 days. Subsequently, they were randomly divided into 10 groups: **F_1** ($n = 3$), **F_2** ($n = 3$), **I_1** ($n = 3$), **I_2** ($n = 3$), **E_1** ($n = 3$), **E_2** ($n = 3$), **P_1** ($n = 3$), **P_2** ($n = 3$), **Cy7 group** ($n = 3$), **DMSO group** ($n = 6$), **saline group** ($n = 3$) and **null group/*ex vivo* group** ($n = 6$).

The mice were maintained in proper cages; one or two groups per cage; 3 to 6 mice per cage (**I_2 + F_2**, **P_2 + E_1**, **E_2 + I_2**, **F_1 + P_1**, **Cy7**, **saline group**, **DMSO group**, **null group**). The mice in each group were marked by one to six bands on their tails with a black permanent marker (OHP marker permanent, alcohol based, waterproof; Centropen, Dačice, Czech Republic) and by ear punch patterns (long term mark).

Subsequently, the mice fur on their back, abdomen and left hind leg was shaved before every imaging experiment (except for day 2 to 4). Firstly, the fur was trimmed using Aesculap® Exacta GT415 (Braun, Kronberg, Germany). Afterwards, the mice were anaesthetized using isoflurane (AErrane® 100%; Baxter Healthcare, Deerfield, USA; 3.0 to 3.5% initial

concentration; 1.0 to 2.0% maintenance concentration, 2.0 L/min air flow) using continuous flow Isoflurane Tec 3 vaporiser (ASA Ltd., Keighley, UK). Their residual fur was removed on the left hind leg and surrounding areas using Veet Silk Fresh^{TM} (thiglycolic acid-containing depilatory cream; Reckitt, Slough, UK) in isoflurane anaesthesia. The excessive depilatory cream was removed after 5-10 min and the mice skin was thoroughly washed with worm tap water and dried by paper towels.

3.5.2. Mice weight measurements

The mice weights were measured on day 1, 2, 3, 4, 7, 11, 15, 18, 28, 57, 85, and 247. The confidence interval (CI) for values 90%, 95%, and 99% (CI_{90}, CI_{95}, and CI_{99}) were calculated with **Equation 8**.

$$CI_{\mathrm{y}} = \bar{x} \pm z_{\mathrm{y}} SD \tag{8}$$

where $\bar{x}$ is the mean value; z is confidence level value (z_{90} = 1.645, z_{95} = 1.96, z_{99} = 2.576), and SD is the standard deviation.

3.5.3. Ultrasound-photoacoustic imaging setup

Multimodal ultrasound-photoacoustic imaging (US-PAI) was performed using Vevo 3100/LAZR-X (ultrasound/photoacoustic) multimodal imaging platform (FUJIFILM VisualSonics, Inc., Toronto, Canada). We used a high-frequency ultrasound Mx400 transducer (30 MHz center frequency, 256 elements linear array, 50 µm axial and 110 µm lateral resolution, FUJIFILM VisualSonics, Inc., Toronto, Canada) equipped with an original jacket for inserting the green narrow optical fibre bundle (14 mm) optical cable (FUJIFILM VisualSonics, Inc., Toronto, Canada) to record the US-PAI of hind limbs in B-Mode and Multiwavelength Mode using Mouse Large Abdominal pre-set. The Time Gain Compensation (TGC) settings was used to see deep within hindlimb tissues by increasing the PAI gain of each pattern (10-55-65-72-75 dB), beginning 9 mm from the upper distance of the transducer surface and proceeding to the bottom hind limb layer at 18 mm (US-PAI field of view 9 to 18 mm).

The mice were anaesthetized with isoflurane (AErrane® 100%; Baxter Healthcare, Deerfield, USA, 3.0% initial concentration; 1.5 to 2.0% maintenance concentration; 1.2 L/min air flow) and fixed in the prone position. Then, their left hind limb (supported with the cellulose square) was positioned to 10 mm from the transducer surface. The space between transducer surface and hind limb skin line was filled by a bubble-free clear transparent ultrasound gel

(OXD, Barcelona, Spain). The feet of the mice were covered in SignaGel Electrode Gel (Parker Laboratories, Inc., Fairfield, USA) to provide a conductive contact with electrodes for ECG monitoring with a build-in ECG monitor, furthermore, their breathing function was monitored with a build-in breathing monitor. All 3D ultrasound records were acquired using a 100 µm step size on a motorized VevoRail system (FUJIFILM VisualSonics, Inc., Toronto, Canada). The spectra were measured at 680, 695, 788, 924, and 970 nm (multiwavelength mode), which enabled to distinguish between deoxyhaemoglobin, oxyhaemoglobin and Cy7 dye (or a labelled polymer).

The US-PAI data acquired during the injections and subsequent scans at time were postprocessed using Vevo LAB V.3.2.5. software (FUJIFILM VisualSonics, Inc., Toronto, Canada). The hindlimb volumes were determined by volumetric analysis in software Vevo LAB.

3.5.4. Polymer administration

The mice were scanned using US-PAI before the administration of solution, during and after the administration of the solution. The mice from groups **F1**, **F2**, **I1**, **I2**, **E1**, **E2**, **P1**, and **P2** were injected with the corresponding polymer in **DMSO** (c_{pol} = 0.10 mg/µL, 5.00 µL). The **DMSO group** and **saline group** (control groups) were injected with pure DMSO (European Pharmacopoeia reference standard; 5.00 µL) or saline (Fresenius Kabi 0,9 %, Fresenius Kabi s.r.o., Praha, Czech Republic; 5.00 µL). Lastly, **Cy7 group** (control group) was injected with 5.00 µL of Cy7-amine hydrochloride solution (1.10 mg was dissolved in 1.000 mL of DMSO and used for Cy7 control group).

These solutions were administered intramuscularly using Vevo Infusion Pump (volume 5.00 ± 0.05 µL; injection speed 1.6 µL/s; FUJIFILM VisualSonics, Inc., Toronto, Canada) using a 0.5 mL insulin syringe (Insulin U100; 0.5 mL; 29G × 1/2", Chirana T. Injecta, Stará Turá, Slovak Republic) while under general anaesthesia. During the administration, mice ECG and breathing were monitored using Vevo 3100/LAZR-X. After the administration, mice were cleaned using cellulose tissues, placed on a plate heater with adjusted temperature (37.7 °C) until the mice regained awareness. Subsequently, they were either placed back into their cages, or they were immediately used in Xtreme measurement (see *chapter 3.5.5*).

The last *ex vivo* biodistribution group served as a control group without any treatment for first 9 days of the experiment (**null group**) – no solution was administered; no measuring procedures were performed (except weight measurements and behaviour observations). Their fur was shaved at the beginning, but not depilated during the first phase. The purpose of this group was

to determine the short-term effect of the intramuscular administration and related procedures on the well-being of the mice. After 9 days (when this group was no longer needed), these mice were used for a different experiment (see *chapter 3.6.*)

3.5.5. Long-term biodistribution monitoring

The fluorescence signal was monitored using Xtreme In Vivo Imaging System (Bruker Biospin, Ettlingen, Germany) with excitation filter 750 nm and the emission filter 830 nm at predetermined timepoints (1-, 5-, 24-, 48-, and 72-hours past administration and then on day 7, 15, 29, 57, 70, 85, 120, 150, 180, and 245). Before measuring abdomen, both sides of the body and right leg of mice were shaved with electric trimmer and hair removal cream (see chapter *3.5.1. General preparation*). The mice were anaesthetized with isoflurane (3.0% initial, 1.5 to 2.0% maintenance concentration) and subsequently the images were acquired (in at least two independent imaging experiments at the given timepoints), the pixel binning was adjusted according to the need.

3.6. Histopathological examination and *ex vivo* experiments

3.6.1. Histological examination

At the end of the long-term experiment (day 202 past administration), one mouse from each group has been sacrificed *via* cervical dislocation (in mild isoflurane anaesthesia). Their organs were visually inspected for abnormalities and samples of their liver, kidneys, hearts, injected thigh muscle and contralateral thigh muscle were collected within minutes after the sacrifice. They were fixed using 4% formaldehyde solution and stored in dark in a refrigerator (4 °C) until processed further.

The samples were washed in PBS and a routine histological examination was performed. Samples were embedding in paraffin and sectioned for 4 or 7 μm histological sections using Leica microtome. Sections were stained using haematoxylin and eosin; representative sections were also stained using Van Gieson Trichrome. The staining was performed according to distributors guidelines (for staining details see **Table S25** and **S26**); Canada balsam was used for slide mounting.

3.6.2. *Ex vivo* experiments

Lastly, the mice (originally in **null group**) were shaved and depilated (identical procedure to the rest of the animals). Subsequently, they were administered with **P2** (c_{pol} = 0.10 mg/µL) or DMSO solutions (5.00 µL). After 6 days, the mice were sacrificed (isoflurane and cervical dislocation) and samples of their muscles (the site of administration) were extracted. The tissues were immediately sliced using McIllwain Tissue Chopper (Stoelting Co., Wood Dale, IL, USA) into 200 µm wide slices, placed into cavity well microscope slides, submerged in corn oil and a coverslip was mounted on top. Immediately afterwards, the samples were visualized using a confocal microscopy.

3.7. Biodistribution data processing

The images from long term imaging (Xtreme imaging, see *chapter 3.5.5*) were processed and the following parameters were observed:

1) **Total signal** in the field of view of the corresponding mice/ organ (sum of all pixels). This value was regarded as **total signal of mice** (I_R)
2) **Number of pixels** with values above predetermined threshold. This value was regarded as **size of depot in mice** (S_R)

The data from long-term biodistribution monitoring were linearized (expressed as natural logarithm of I_R or S_R). The data corresponding to **Phase 2** (see *chapter 4.5.1*) were fitted with linear functions in OriginPro 8.6.0 (OriginLab Corporation, Northampton, MA, USA). The biological half-lives ($t_{1/2}$) were calculated with **Equation 9**:

$$t_{1/2} = \frac{\ln 2}{k} \tag{9}$$

The results can be seen in **Table S24**, **Figures S70** to **S87**.

4. Results and Discussion

4.1. Polymer selection

The polymers were selected for this study because they are non-ionic homopolymers of acrylamide *N*-derivatives with one or two alkyl moieties, and their aqueous solutions display LCST thermoresponsiveness with various T_{CP}s at similar polymer concentrations (**pAP** ≫ **pNIPAM** ≈ **pDEA** > **pDFEA**; **Figure 10**).[6,127] While **pAP**, **pNIPAM**, **pDEA** have been studied extensively,[6,8] **pDFEA** is a relatively new and atypical thermoresponsive acrylamide with fluorine atoms.[127] As polyacrylamides, all four polymers act as hydrogen bond acceptors, but both **pDFEA** and **pNIPAM** can also act as hydrogen bond donors because they contain amide moieties. In addition, **pDFEA** contains -CF_2H moieties, *i.e.*, lipophilic hydrogen donors[128] (see **Scheme S2** and *Chapter S8.2.*). All these polymers are non-toxic and biocompatible as well. Accordingly, their different properties (*e.g.*, hydrophilicity or T_{CP}) may be used to tailor the final materials for biomedical applications.[6,127] Nevertheless, we avoided comparing copolymers because their T_{CP} depends on the content of their individual monomers and on their architecture, thus adding other unknown variables to the equation.[129]

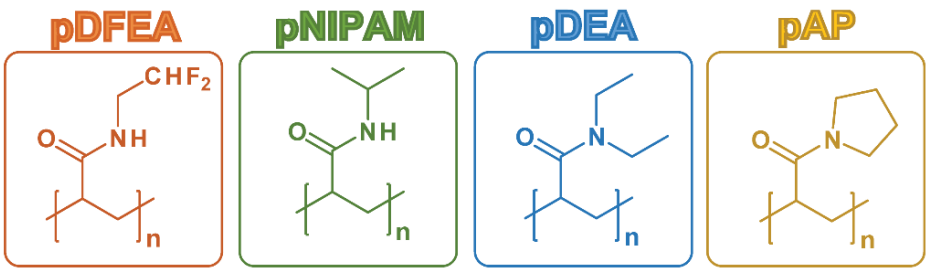

Figure 10. Structures of the study polymers: poly[(*N*-2,2-difluoroethyl)acrylamide] (**pDFEA**), poly[(*N*-isopropyl)acrylamide] (**pNIPAM**), poly[(*N*,*N*-diethyl)acrylamide] (**pDEA**), and poly[(*N*-acryloyl)pyrrolidine] (**pAP**).

We targeted polymers with properties suitable for biomedical applications. For this reason, **pDFEA**, **pNIPAM**, **pDEA**, and **pAP** had a narrow molecular weight distribution ($Đ_M \leq 1.11$) and molar masses in three different ranges (≈ 20 to 25 kg/mol, ≈ 30 to 35 kg/mol and ≈ 40 to 50 kg/mol) but all molar masses are lower than the renal excretion limit[71,130,131] so that they would not accumulate in the body.[130] The end groups of these polymers contained a methyl ester (from methyl acrylate) on one end and a carboxyl group (initiator residue) on the other, which can be conveniently used to introduce tracers, dyes, and other moieties.

4.2. Polymer synthesis, modifications, and characterization

We prepared these four polymers *via* controlled reversible addition-fragmentation chain-transfer (RAFT) radical polymerization[125] (**Figure 11**) using 4-cyano-4-[(dodecylsulfanylthiocarbonyl)sulfanyl]pentanoic acid as the CTA and 4,4′-azobis(4-cyanovaleric acid) (ACVA) as the initiator (see **Table 1** for the initial quantities of the reagents). After the polymerization, the polymers ending with CTA were mixed with propylamine (aminolysis of the terminal CTA)[125] and then with an excess of methyl acrylate (to mask the reactive thiol moiety by Michael addition),[125] as shown in **Figure 11** and **Table 2**. Lastly, we purified and characterized these polymers by SEC and NMR spectroscopy to determine their purity and to confirm CTA removal (see *chapter S8.3.*). The properties of these polymers are outlined in **Table 4**.

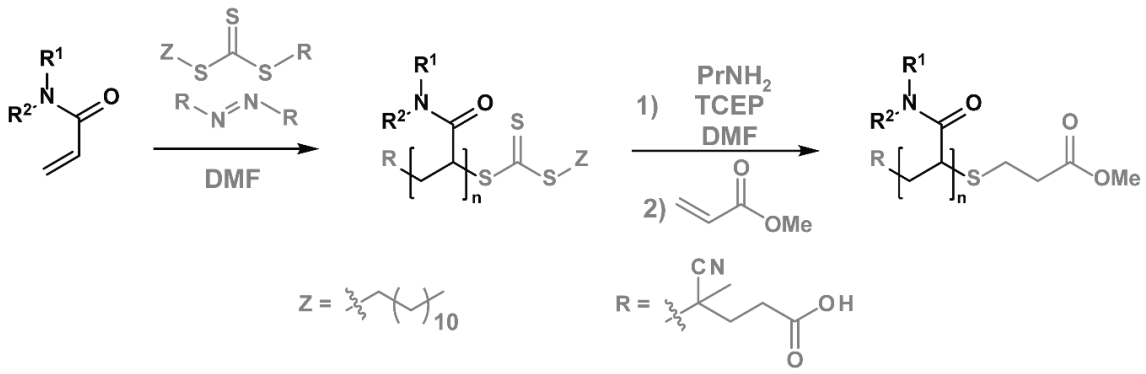

Figure 11. Polymer synthesis and subsequent modifications

Table 4. Polymer characteristics after removal of CTA

Polymer		M_w[a] (kg/mol)	M_n[a] (kg/mol)	$Đ_M$[a]	Yield[b] (%)	d*n*/d*c*[c] (mL/g)
pDFEA	**F1**	26.2	24.2	1.08	68.3	0.088 ± 0.003
	F2	36.2	35.1	1.03	79.7	0.092 ± 0.005
	F3	49.6	46.9	1.06	79.5	0.095 ± 0.004
pNIPAM	**I1**	20.2	19.6	1.03	50.6	0.167 ± 0.018
	I2	31.6	30.8	1.03	58.1	0.151 ± 0.012
	I3	48.4	45.2	1.07	55.6	0.143 ± 0.013
pDEA	**E1**	22.3	21.2	1.06	60.5	0.171 ± 0.004
	E2	34.7	31.7	1.09	61.3	0.176 ± 0.011
	E3	41.3	37.5	1.10	57.5	0.145 ± 0.010
pAP	**P1**	19.6	17.6	1.11	86.0	0.192 ± 0.007
	P2	36.0	32.9	1.09	77.7	0.180 ± 0.015
	P3	51.2	46.3	1.11	79.1	0.164 ± 0.007

[a]Determined by SEC; [b]polymerization yield after the purification procedure based on monomer weight; [c]determined by differential refractometry in PBS at 29 °C and 620 nm in PBS

4.3. The effect of PBS and FBS on the T_{CP}

The T_{CP}s of our thermoresponsive polymers are either known (for **pNIPAM**[16–20,26,27,45,46], and **pAP**[20]) or expected (for **pDFEA** and **pDEA**) to be lower in physiologically relevant solutions (FBS and PBS) than in pure water because these buffered solutions have a higher pH and ion concentration (as discussed in the introduction). However, these polymers also have terminal carboxylic moieties ($pK_a \approx 4.8$), and while they are almost exclusively dissociated at neutral pH, unbuffered water dissolves atmospheric carbon dioxide,[35] lowering the pH to values near the pK_a of these carboxylic acid (**Table S7**). As a result, the carboxylic groups will no longer be fully deprotonated, decreasing the hydrophilicity[15,35] and T_{CP} of these polymers.[35] In contrast, both PBS and FBS (140 mM; pH = 7.4) reliably maintain the pH and osmotic pressure at physiological values.[122,132]

Considering these differences, we have compared the effect of different solvents (water, Dulbecco's PBS[122] and FBS) on T_{CP} (c = 10.0 mg/mL; **Figure 12**). In line with previous studies, most T_{CP} values of our polymers were higher in pure water than in PBS[16–20,23,26,27,45] and FBS[16,26] because the ions and proteins of buffered solutions lower the T_{CP} of these polymers. Since differences in T_{CP}s between solvents may be significant for many applications, polymers should be tested in an environment as similar as possible to that of the intended application.

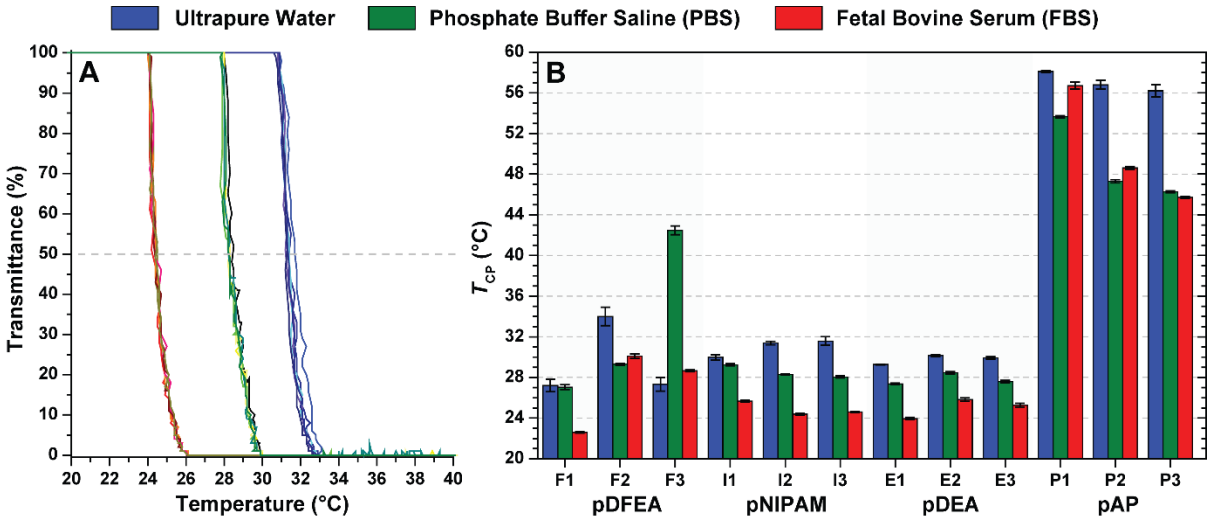

Figure 12. (**A**) Comparison of 6 turbidimetric measurements of **I2** (**pNIPAM**) in water, PBS and FBS (c = 10.0 mg/mL); (**B**) T_{CP} of all polymers in water, PBS and FBS (c = 10.0 mg/mL) expressed as a mean of 6 measurements ± standard deviation. The results indicate a shift in T_{CP}.

4.4. Determination of T_{CP} by DLS

As shown in Figure 12 B, the T_{CP} of **pDFEA** with the highest molar mass (F3) was much higher in PBS than in water. To understand the unexpected T_{CP} of this polymer, as measured

by turbidimetry, we assessed polymer aggregation as a function of temperature (10 to 50 °C) by DLS, in PBS, at a concentration of 10.0 mg/mL (**Figure S42** to **S53**). Unlike most samples, **pDFEA** polymers showed two major changes in population size with the increase in temperature (**Figure S42** to **S44**). The first change (at 26 to 30 °C) can be ascribed to unimer aggregation (radius 20 to 100 nm), and the second (from 40 to 50 °C) to aggregate coalescence into even larger polymer assemblies (radius 1000 nm or larger). Thus, turbidimetry detects the first thermal change in most samples, but only the second in **F3**.

Long **pDFEA** (co)polymers, such as **F3**, may form non-typical nanogel-like aggregates with low polymer concentrations, as shown in our previous studies.[81–83] In these particles, the aggregation causes only a minor local increase in polymer concentration. When combined with the low d*n*/d*c* of the solute (**Table 4**), this increase in polymer concentration accounts for the small difference in refractive indices between the phase-separated polymer and the bulk solution, which may prevent an accurate determination of T_{CP} by turbidimetry.[42] Upon further heating, these nanogel-like particles aggregate/ coalesce, increasing the turbidity. Therefore, discrepancies in turbidimetric measurements may be explained by differences in the architecture of polymer aggregates and by the low d*n*/d*c* of **pDFEA**.

4.5. The effect of PBS and FBS on T_{CP} as a function of polymer concentration

Proteins (in FBS) can affect the T_{CP} of polymers indirectly ('non-specifically', *i.e.*, by competing with polymers for its solvation as well as by excluded volume/crowding effect[17,29]) or directly ('specifically', *i.e.*, by forming complexes with the polymers[17,30]).[17] In turn, inorganic salts (in PBS and FBS) can also indirectly interfere with polymers by interacting with and destabilizing their solvation shell, thus decreasing their solubility and T_{CP} (Hoffmeister effect), regardless of the polymer concentration.[16,23] Unlike inorganic salts, however, proteins affect T_{CP} as a function of polymer concentration, as shown by our results (**Figure 13**).

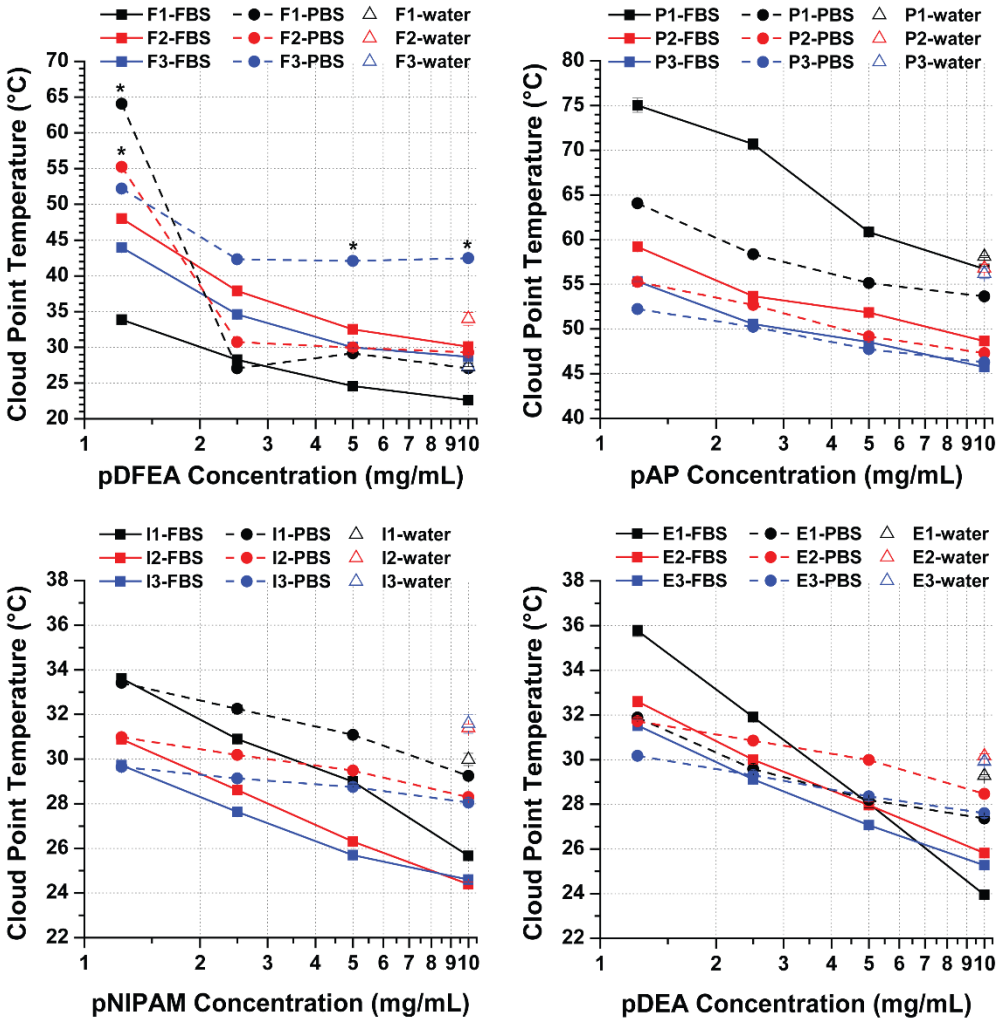

Figure 13. Plot of T_{CP}s of the polymers **pDFEA** (top-left), **pAP** (top-right), **pNIPAM** (bottom-left) and **pDEA** (bottom-right) in FBS and PBS as a function of polymer concentrations. All T_{CP}s are expressed as the mean of 6 measurement cycles ± standard deviation. Asterisks (*) indicate potential outliers.

At low polymer concentrations, polymers form soluble protein-polymer complexes (protein binding) in FBS, which prevent them from aggregating, thereby increasing their T_{CP} above that of PBS solutions, as observed in **pDEA** and **pNIPAM** (at both low and high **pAP** concentrations). Because the polymer-binding capacity of proteins is limited (albeit very high for **pAP**), this effect is only detected at low polymer concentrations and decreases with the increase in polymer concentration (until being offset by 'non-specific' effects, which decrease the T_{CP}).

At high polymer concentrations, in contrast, proteins predominantly have a 'non-specific' effect by competing with polymer chains for solvation with the polymer[16,17,23,24,133] (similarly to inorganic ions), thereby facilitating aggregation and lowering the T_{CP}s. Proteins may also

stabilize polymer aggregates *via* hydrophobic interactions, further lowering the T_{CP}s. Under such conditions, most polymers in FBS have the lowest T_{CP}s of all three media tested in this study (except for **F3** in PBS, as discussed above).

For the purpose of this analysis (**Figure 13**), we disregarded the T_{CP} of the highest polymer concentrations (20.0 and 40.0 mg/mL) because they differed considerably between independent measurements (low reproducibility), not only in FBS but also in PBS. Nevertheless, the complete dataset is provided in **Tables S3** to **S6**. Furthermore, in the range used in this analysis (1.25 to 10.0 mg/mL), except for a few outliers, all three molar masses of each polymer showed similar T_{CP} trends, that is, T_{CP} decreased with the increase in polymer concentration, in line with previous studies.[6,17–20]

4.6. The effect of PBS and FBS on polymer aggregation

LCST polymer aggregation is an entropy-driven endothermic process[6,8,42] affected by surrounding ions/ proteins. Adding ions/ proteins can induce conformational changes in the polymer (aggregation) or affect its solvation shell, both of which can be detected as heat effects.[6,134–136] A decrease in enthalpy after adding ions/ proteins indicates an enthalpic effect, *i.e.*, polymers interact with ions/ proteins (or new strong polymer-polymer interactions are formed). Conversely, an increase in enthalpy after adding these ions/ proteins indicates an entropic effect, *i.e.*, the loss of specific interactions, thereby increasing the entropy, *e.g.*, due to the loss of the solvation shell.[136]

Considering the above, we assessed the interaction enthalpy of **pDFEA**, **pNIPAM**, **pDEA**, and **pAP** with PBS and FBS by isothermal titration calorimetry (ITC), which revealed a complex titration isotherm[90] (**Figure 14B**), with three phases: **I**, **II** and **III** (**Figure 14A**). In **phase I**, the heat flux can be ascribed to the neutralization of the terminal carboxylic acid because adding 3 to 5 µL of PBS (pH = 7.41) or FBS (pH = 7.46) to the solution of benzoic acid had a similar effect on the heat flux (**Figure S41**). For this reason, the corresponding data points were excluded from the titration isotherms. Subsequent adding of titrant induced exo- or endothermic processes, which strongly depended on the titrant concentration (**phase II** on the titration isotherms). After the critical concentration of titrant (**Figure 14B**), a non-zero heat flux, weakly dependent on the titrant, was still detected (**phase III**). Based on these results, we focused on the heat flux from **phase II** to analyse the solvent-polymer interactions.

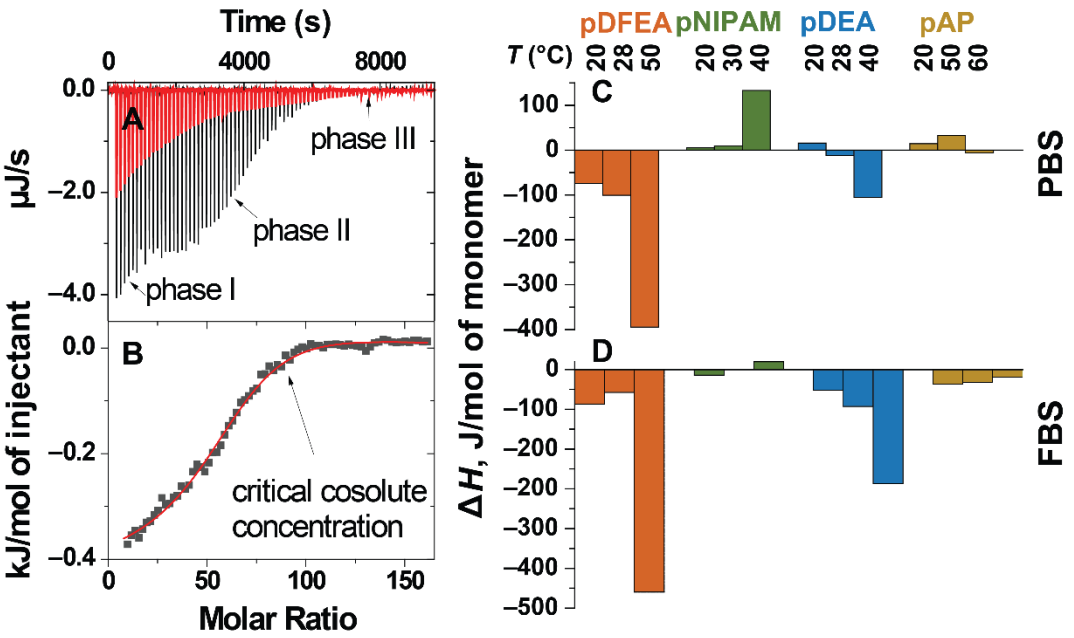

Figure 14. ITC – Titration of PBS to water (blank, red line) (**A**), titration of PBS to polymer **F3** (**pDFEA,** ***c*** = 10.0 mg/mL in ultrapure water,black line) (**A**); integrated heat, normalised to 1 mol of **F3** injectant (scatter), fit to model (line) (**B**). Enthalpies of the titration of polymer solutions (*c* = 10.0 mg/mL) with PBS (**C**) and FBS (**D**), normalised to 1 mol of monomeric units at three different temperatures. The values of enthalpies are outlined in **Table S5**.

In non-aggregated polymers (at low temperatures), adding PBS to the solution had a positive enthalpic effect on **pNIPAM**, **pAP** and **pDEA**, as expected based on the Hoffmeister effect, but surprisingly had a significantly negative enthalpic effect on **pDFEA**. On the one hand, PBS decreases the solvation shell of all polymers (positive enthalpic effect). On the other hand, PBS increases polymer-polymer bonds in the aggregates (negative enthalpic effect). Since PBS had a net negative enthalpic effect on **pDFEA**, **pDFEA** must have strong intramolecular interactions (possibly due to hydrogen bonding between CF_2H moieties[128]).

In aggregated polymers (at high temperatures), PBS had a negative enthalpic effect on **pDFEA**, **pDEA** and **pAP**, indicating that this buffer promotes the formation of enthalpically favourable polymer-polymer interactions. However, adding PBS to **pNIPAM** had a positive enthalpic effect, suggesting further dehydration resulting from salting out. Overall, PBS disrupts the solvation shell of thermoresponsive polymers, thereby promoting aggregation.

Adding FBS to both non-aggregated and aggregated polymers (at both low and high temperatures) had a more negative enthalpic effect than adding PBS due to the additional strong polymers-proteins interactions (**Figure 14**). The amphiphilic proteins in FBS may bind to polymers and polymeric aggregates[16,58] *via* hydrophobic interactions[56,58] and thus stabilize

them. In all polymers, adding FBS to polymer aggregates had a stronger negative enthalpic effect than adding FBS to non-aggregating polymers, possibly because polymer aggregates are more prone to interact with proteins through the hydrophobic interactions. Consequently, FBS stabilizes thermoresponsive polymer aggregates more strongly than PBS.

4.7. *In vitro* biological study

To evaluate the safety of the polymers, we investigated the polymers' cytotoxicity using human fibroblast (HF) and rat mesenchymal stem cell (rMSC). The HF were selected as model cells because they are common in muscles, and because they participate in extracellular matrix synthesis. The rMSC were chosen as a highly sensitive model of normal healthy cell. The results of *in vitro* cytotoxicity study are depicted in **Figure 15**. Within the tested polymer concentrations, no polymer decreased the cellular viability below 70% (threshold for cytotoxicity).[91] Additionally, we observed no significant difference between the viabilities of study groups (the cells treated with the polymers) and control group (untreated cells). Therefore, in line with previous results,[127] our polymers are non-cytotoxic.

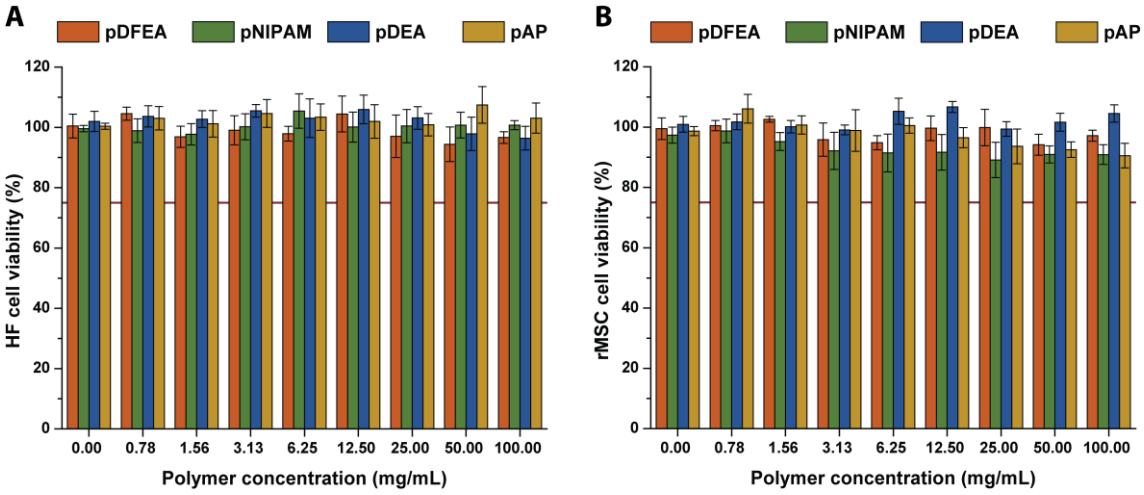

Figure 15. Viability of human fibroblast (HF; **A**) and rat mesenchymal stem cell (rMSC, **B**) as a function of polymers (**F3**, **I3**, **E3**, and **P3**) concentration. All cells were incubated for 72 hours with study polymers; the cell viability was determined using resazurin assay.

4.8. Polymer conjugation with fluorescent dye

The polymers **F1**, **F2**, **I1**, **I2**, **E1**, **E2**, **P1**, and **P2**, were labelled with fluorescent dye (Cy7-amine, see **Figure 16**). This dye is chemically and biologically stable fluorescent dyes with high extinction coefficients. Cy7-amine (λ_{ex} = 756 nm; λ_{em} = 779 nm) was selected as a label *in vivo* biodistribution experiments because of its high excitation and emission wavelengths.

Afterwards, we purified the polymers with two consequent preparatory SEC. Then, we determined the polymer purity using SEC (the presence of unreacted fluorescent dye; **Figure S67** and **S68**) and the amount of polymer-bound dye spectrophotometrically (**Table 5**).

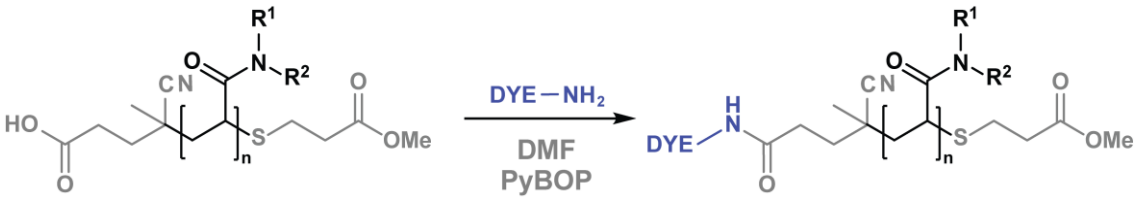

Figure 16. The polymer modification/ polymer labelling with the fluorescent dye.

Lastly, we determined the *in vitro* chemical stability of the fluorescent label in GPC buffer. Over the course of 200 hours, no significant increase of non-bound dye was observed, which indicates that our polymers are suitable for pharmacokinetics observations.

Table 5. Molar amount of Cy7 (n_{Cy7}) and ratio of n_{Cy7}/n_{pol} were calculated from spectrophotometry. The polymer purity was determined as a ratio of polymer peak and other peaks integrals in SEC and HPLC.

Polymer		**purity** (%)	$\boldsymbol{n_{Cy7}}$ (μmol/mg)	$\boldsymbol{n_{Cy7}/n_{pol}}$
pDFEA	**F1**	≥ 99.5	24.5 ± 0.9	0.59 ± 0.02
	F2	≥ 99.5	13.6 ± 0.7	0.48 ± 0.03
pNIPAM	**I1**	≥ 99.5	13.4 ± 0.7	0.26 ± 0.01
	I2	≥ 99.5	11.8 ± 0.5	0.36 ± 0.03
pDEA	**E1**	≥ 99.5	3.1 ± 0.4	0.06 ± 0.01
	E2	≥ 99.5	4.5 ± 0.4	0.14 ± 0.02
pAP	**P1**	≥ 99.5	14.3 ± 0.7	0.25 ± 0.01
	P2	≥ 99.5	8.6 ± 0.6	0.27 ± 0.02

4.9. *In vivo* biological model

The BALB/c mice were randomly divided into 8 study groups: **F1**, **F2**, **I1**, **I2**, **E1**, **E2**, **P1**, **P2**, and 4 control groups: **Cy7**, **DMSO**, **saline group** and **null group**. The mice from study groups were injected with a solution of the corresponding Cy7-labelled polymer in DMSO into the thigh of their hind left legs. Although all study polymers are water soluble and, therefore, could be administered in their aqueous solutions, we decided to administer the polymers in their DMSO solutions. By using the DMSO solutions, we prevented the polymers from aggregating in the syringe/ needle during the administration (particularly in **pDFEA**), which would result in uneven distribution of depot, hindering the determination of the polymer pharmacokinetics. **Cy7 group** was injected with solution of Cy7-amine in DMSO to investigate the pharmacokinetics of this dye (whether this dye would accumulate in the study tissues). Then, **DMSO** and **saline groups** were injected with DMSO or saline, respectively; these groups served as control groups to investigate the effect of intramuscular administration of solvent on the tissues. Lastly, **null group** was not injected with any solution – we used these mice to investigate the effect of intramuscular administration on the mice behaviour and feeding patterns.

The mice were anaesthetized with isoflurane and their fur was trimmed and removed using hair removal product to increase the sensitivity of photoacoustic imaging techniques. After the administration, the polymer depot in the hind legs of was often scanned using fluorescence imaging; the selected mice as a function of time were depicted in **Figure 17**.

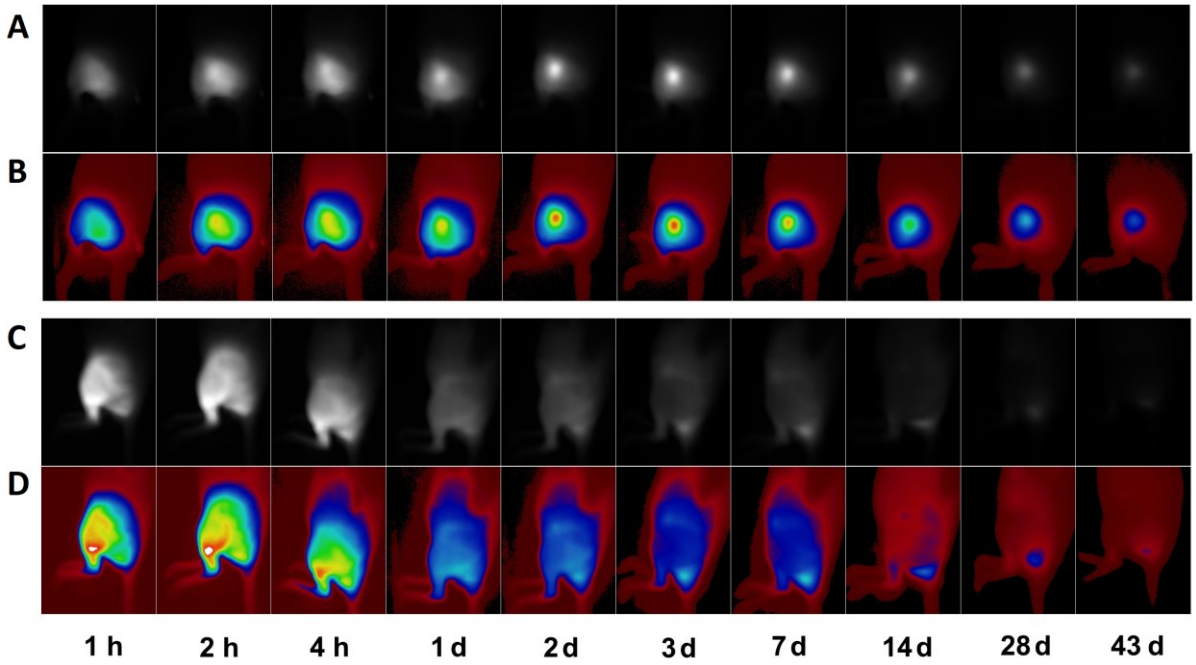

Figure 17. Images from fluorescence imaging. Fluorescence imaging signal was depicted in grayscale (**A**, **C**) and as colour gradient, merged with white light image of the mice (**C**, **D**). The mice were administered with the polymer **I2** (**A**, **B**) or **P2** (**C**, **D**).

4.10. Determination of polymers pharmacokinetics

The images from fluorescence imaging were processed and the following two quantities were evaluated:

1) **Total signal of polymer (I_R)** in the field of view of the corresponding mice/ organ (sum of all pixels). This quantity is proportional to the amount of the labelled polymer in the depot.
2) **Size of depot in mice (S_R)**. This value was calculated from the number of pixels above a specific threshold (identical for all images).

Both study parameters (I_R, and S_R) change as a function of time; the development may be divided into 3 phases (**Figure 19**):

Phase 1 (depot maturation). This phase begins immediately after the polymer administration and lasts approximately 3 days[13] (up to 10 days in **pDFEA**). During this phase, the polymer diffuses through the tissue, which results in the increase of S_R. Additionally, this diffusion may increase the fluorescence signal (I_R): initially, the polymer is very concentrated, therefore, a portion of signal is lost due to auto-absorption, however, this auto-absorption decreases with more diluted depots. The signal reaches maximum at t_{max}, which was considered as a start of the **Phase 2**. In our previous article, we have shown, that only a portion of polymer becomes tissue-bound (and thus enters **Phase 2**), while the rest is eliminated into bloodstream.[13] As a result, the polymer signal should decrease quickly during the first 2 days and then decrease

slowly over several weeks (**Phase 2**).[13,70] Nevertheless, we were unable to observe the initial decrease of signal because this decrease of signal was less pronounced than the signal increase caused by the depot redistribution.

Phase 2 (depot dissolution). This phase lasts for several weeks to months. During this phase, both I_R and S_R decreased with time relatively slowly and follows the 1st order kinetics. This phase may be ascribed to the dissolution tissue-bound polymers, as suggested in our previous article.[13]

Phase 3 (final phase). This phase begins several months after the administration but can be clearly seen only in some polymers. During this phase, both I_R and S_R decrease very slowly (if at all), and the decrease no longer follows the 1st order kinetics. In this phase, the major source of signal is the autofluorescence of mice.

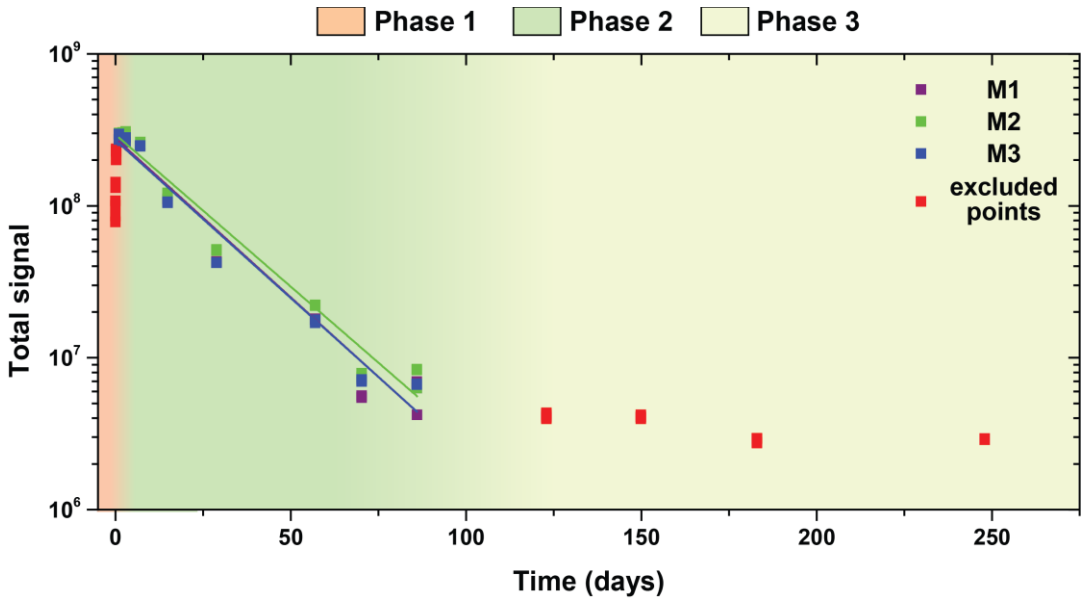

Figure 18. The total depot signal as a function of time during **Phase 1**, **2**, and **3**.

Considering the above, we fitted the data in **Phase 2** with monoexponential functions to determine the pharmacokinetics of the study polymers (**Table 6** and **S6**, **Figure S70** to **S87**). The biological half-lives varied from 15 days to 5 months across polymers: the shortest half-lives were observed in **pAP**, the longest in **pDFEA**. The approximate $t_{½}$s of our polymers corroborate those in previous studies.[13,70] In line with our previous study, the order or $t_{½}$s of study polymers (**pAP** ≤ **pDEA** < **pNIPAM** ≪ **pDFEA**) inversely correlates with their T_{CP}s (**pAP** ≫ **pDEA** ≈ **pNIPAM** > **pDFEA**).[13] However, noticeably, even though **pDEA** and **pNIPAM** have similar T_{CP}s, the biological half-lives of **pNIPAM** are much higher than those of **pDEA**. This result suggests that the T_{CP} is not the only factor that influences the $t_{½}$ of the polymer – the $t_{½}$ may be influenced by protein binding (hydrogen bonds in **pNIPAM** and

pDFEA may increase the $t_{½}$). Interestingly, molar mass of the study polymers had only a minor effect on the overall biological half-lives ($t_{½}$ increases with molar mass). Our results show that biological half-lives of polymers may be tuned by choice of thermoresponsive polymer, and as shown in our previous articles,[13] fine-tuned by choice and content of co-monomers.

Table 6. Calculated parameters of polymer release: time of maximum signal (t_{max}), biological half-lives ($t_{½}$), and fitting R^2; all parameters were calculated both from signal and depot size as a function of time. The results are depicted as mean ± mid-range.

Polymer		Total signal		Depot area	
		t_{max} (d)	$t_{½}$ (d)	t_{max} (d)	$t_{½}$ (d)
pDFEA	**F1**	≈ 1.0	155 ± 44	2 ± 1	168 ± 85
	F2	2 ± 1	145 ± 22	2 ± 1	151 ± 43
pNIPAM	**I1**	2 ± 1	52 ± 12	2 ± 1	98 ± 32
	I2	2 ± 1	60 ± 11	2 ± 1	103 ± 11
pDEA	**E1**	2 ± 1	15 ± 1	2 ± 1	28 ± 3
	E2	2 ± 1	22 ± 3	2 ± 1	35 ± 14
pAP	**P1**	2 ± 1	16 ± 5	2 ± 1	27 ± 5
	P2	2 ± 1	15 ± 1	2 ± 1	26 ± 6
Cy7		< 0.5	5 ± 2	< 0.5	9 ± 3

In all polymer-treated mice (most pronounced in **pAP**) as well as Cy7-treated mice, we temporarily observed polymer signal in mice kidneys and livers, even though no polymer was administered directly into these organs (**Figure 19**). No signal can be detected immediately after the administration; the signal peaks approximately 2 days past administration and slowly diminishes in 2 to 3 weeks. This secondary accumulation of signal can be ascribed to an accumulation of blood-carried polymer in these organs after the polymer administration. Although we did not determine the fate of polymers on the cellular level, the polymer is most likely uptaken by Kupffer cells (in liver) and mesangial cells (in kidney) with pronounced phagocytosis ability.[137] The liver and kidneys of BALB/c mice are among the organs with the highest perfusion rates: more than 40% of blood flows through the liver and around 15% flows through the kidneys (**Table 7**).[138] Other organs with high blood flow and perfusion rates, *e.g.* brain, lungs, and myocardium are probably too shielded by the surrounding tissues (*e.g.* brain), too diffuse and the signal is hindered by noise (*e.g.* lungs), the depot is too small to be visualized or does not contain enough polymer.

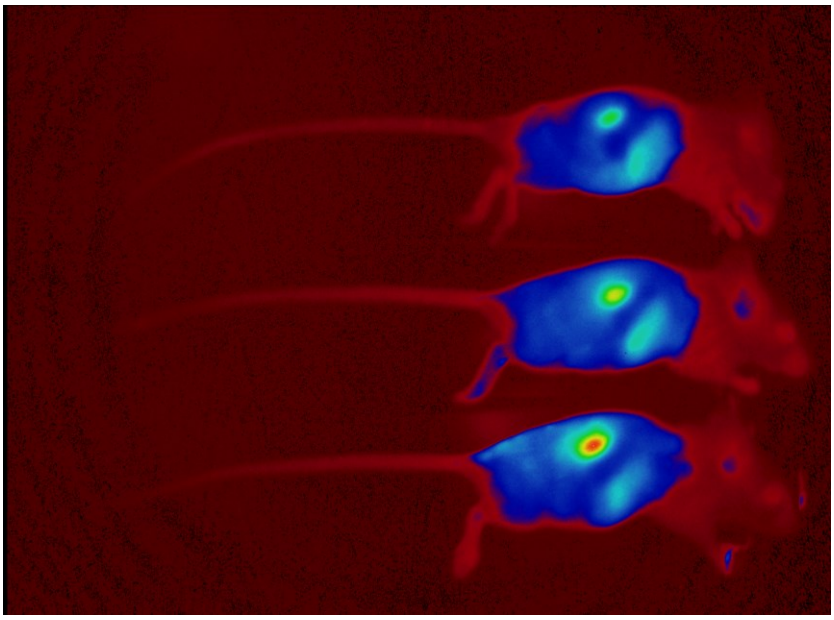

Figure 19. Mice from **P1 group**, 48 hours past polymer administration, lying on their left side. The upper-left depot can be ascribed to accumulation of polymer in their kidneys; the lower-right depot corresponds to polymer accumulation in liver.

Table 7. Acute blood flow of major organs of the BALB/c mice, adapted from literature.[138]

Organ	**Absolute blood flow** (μL/min)	**Blood flow per kg of organ** (ml/kg/min)	**Relative blood flow** (% of total)
liver	945 ± 242	95 ± 20	49 ± 19
kidneys	418 ± 44	131 ± 7	15 ± 5
brain	387 ± 51	93 ± 15	18 ± 5
lungs	250 ± 27	145 ± 23	12 ± 3
myocardium	137 ± 7	106 ± 6	6.7 ± 1.4
spleen	46 ± 8	47 ± 8	2.2 ± 0.7
thymus	23 ± 2.5	81 ± 7	1.1 ± 0.3
mesenterial lymph node	23 ± 3	58 ± 7	1.1 ± 0.3
adrenal grands	15 ± 3	306 ± 59	0.7 ± 0.3
ovaries	8 ± 2.7	156 ± 37	0.4 ± 0.2
total	2252 ± 390	N/A	100

Although the signal from the secondary depot in kidneys is slightly higher than that in liver, the signal ratio cannot be directly translated into the ratio of deposited polymer, because liver is situated in a greater depth than the kidneys in mice and therefore the signal from liver experiences more shielding. Therefore, we estimate that the amount of polymer deposited into the liver might be higher then in kidneys. However, the data is insufficient to further support this hypothesis.

Based on these results and the results from previous studies,[13,70,71] we proposed a physiological biodistribution model (**Figure 20**). After the administration, a portion of polymer (characterized by factor *A*) binds to tissue and therefore eliminates relatively slowly (following first order kinetics), while the non-tissue bound polymer is eliminated approximately 3 to 10 days. The blood-borne polymer can secondarily temporarily accumulate in both liver and kidneys, from where it is eliminated into bile or urine.

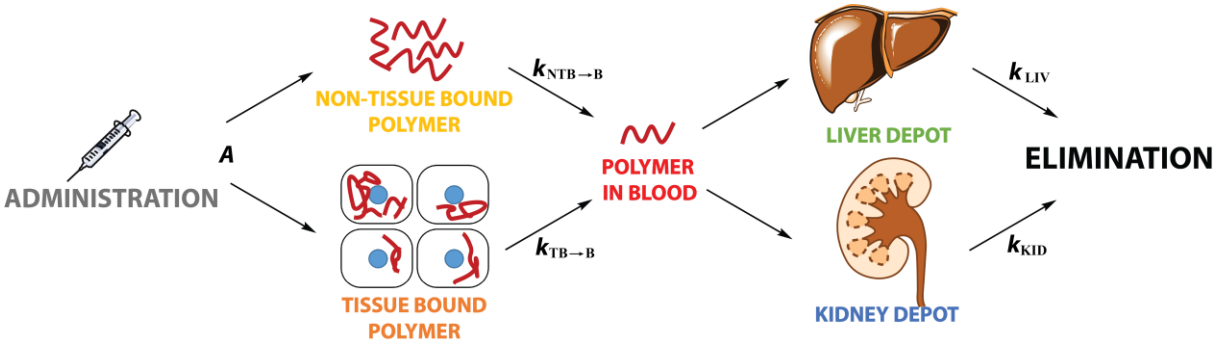

Figure 20. The proposed biodistribution model for thermoresponsive polymers. The kinetics is characterized by A (fraction of administered polymer becomes tissue bound); $k_{\mathrm{NTB\rightarrow B}}$ (dissolution constant of the non-tissue bound polymer), $k_{\mathrm{TB\rightarrow B}}$ (dissolution constant of the tissue bound (intracellular) depot), k_{LIV} (dissolution constant of the liver depot), and k_{KID} (dissolution constant of the kidney depot).

4.11. Mice weights as an indicator of their health

We observed the weights of mice as a function of time, because some pathologies or discomfort may lead to decrease (less commonly increase) of mice weights. The weights of the testing groups (**F1**, **F2**, **I1**, **I2**, **E1**, **E2**, **P1**, and **P2**) were compared to the control groups (**Cy7**, **DMSO**, **saline**, and **null groups**), see **Figure 17** and **S69**. Although a few outlier points can be seen (*e.g.* in **P1**, but these mice were slightly lighter from the beginning of the experiment), the overall trend of all mice weights were similar and physiological. We observed no weight gain retardation or even weight loss, indicating the fitness of study mice.

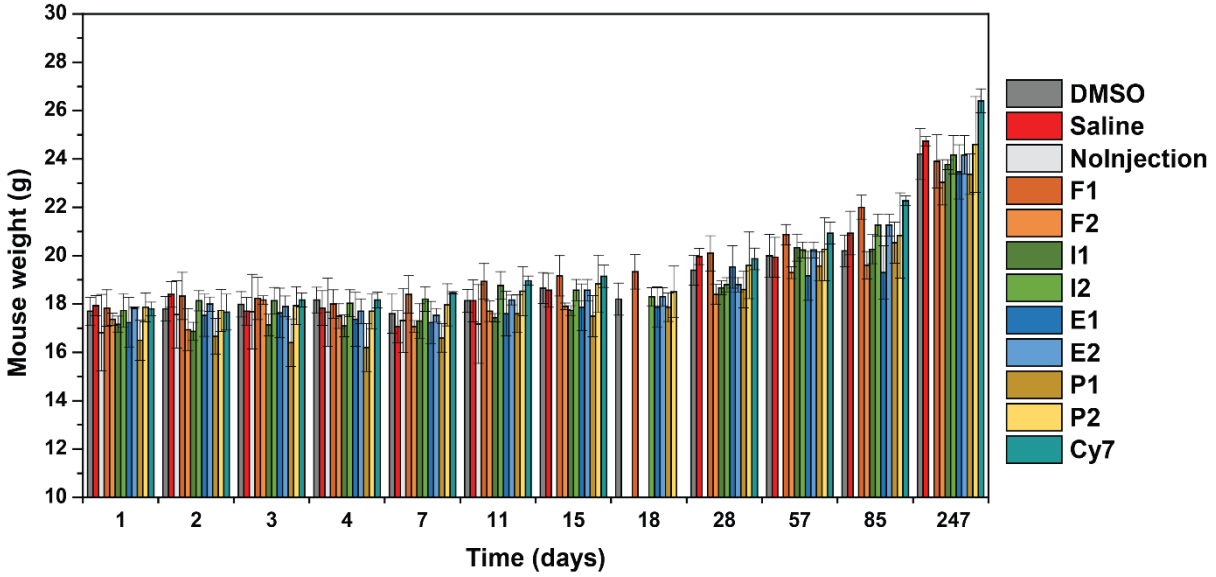

Figure 21. Weights of the mice from all groups as a function of time

The **null group** (no compound was administered, but the remaining treatment was identical to the that in other mice) was included in the study to investigate the effect of solution administration. We observed no significant deviation of weights of this group from the rest of the groups, indicating that the administration had only minor (if any) effect on the mice fitness. Then, 11 days past the beginning of the experiment, the mice were used for ***ex vivo*** **experiment** (*4.5.3. Ex vivo polymer distribution*) because this mice group was no longer needed.

4.12. *Ex vivo* biological study (histological examination)

At the end of the experiment (day 202 past administration), one mouse from each group was sacrificed *via* cervical dislocation (in isoflurane anaesthesia) and their cadavers were thoroughly inspected *ex vivo*. Afterwards, the samples of their muscle (both injected and contralateral), kidneys, livers, and hearts were collected, and histological examinations were performed with haematoxylin & eosin stain and, in some samples, also with Van Gieson stain (**Figure 18**). Apart from minor sign of fibrosis in some glomeruli seen in all mice (including control group) that can be ascribed to mice age, no sign of pathology or chronic toxicity was found in any organ.[139,140] All differences between study groups can be ascribed merely to differences in sampling and staining (most pronounced in muscle). A thorough description of all findings of all samples can be seen in ESI (*chapters S15 and S16*).

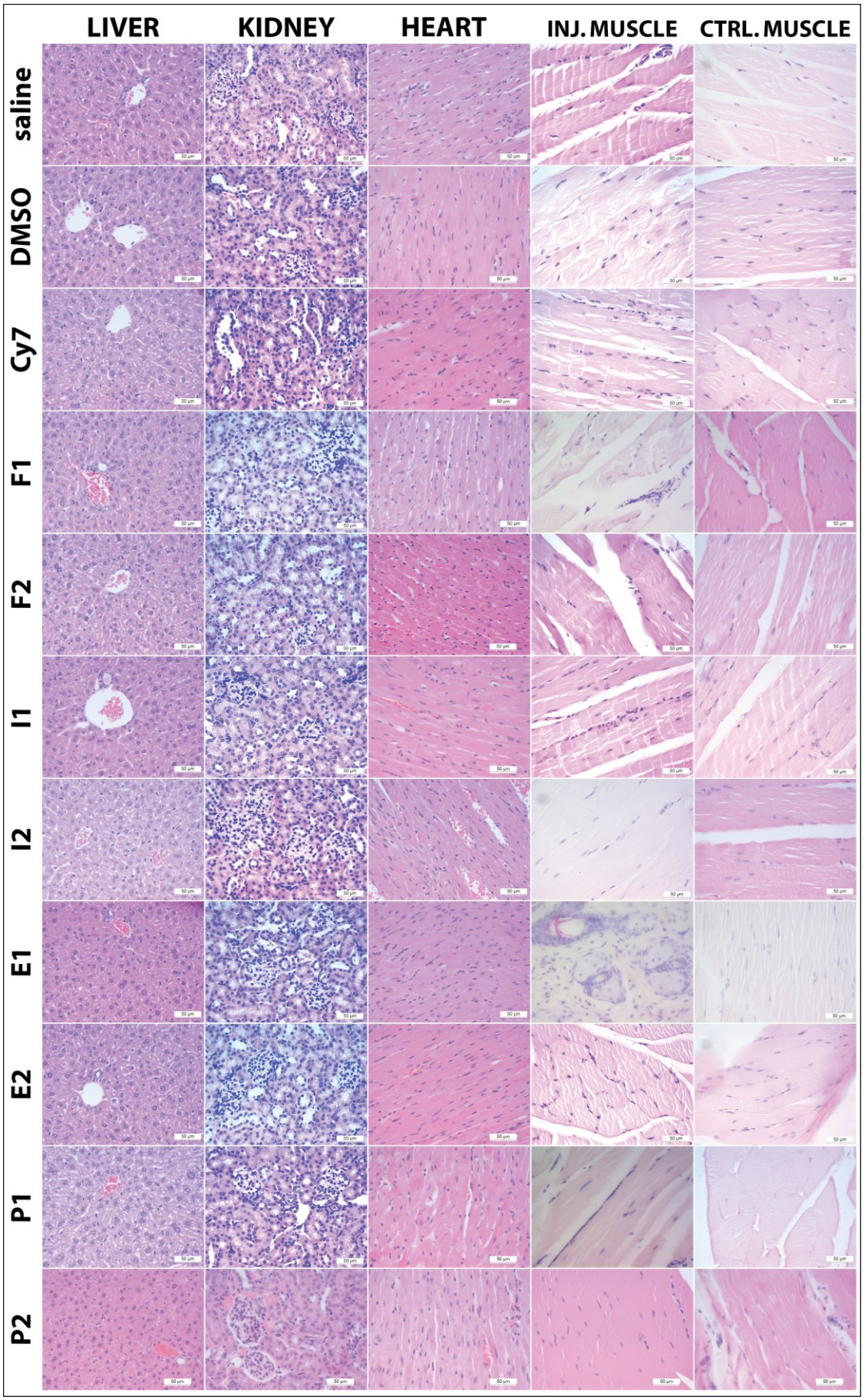

Figure S22. Histological examination of mice (202 days past administration).

4.13. *Ex vivo* polymer distribution

Additionally, we performed an *ex vivo* histopathological examination of the injection site 6 days after administering the polymer to investigate the depot distribution on microscopic level. However, observing the polymer was difficult, because the polymers are soluble in water and alcohols, thus it would dissolve in aqueous/ methanolic fixing or staining solutions. Therefore, we were unable to fix or stain the study tissues properly. As a result, the samples needed to be processed very quickly to avoid autolysis (due to lack of tissue fixation); furthermore, we could not stain the structures.

Nevertheless, we administered the **P2** solution into the thigh of mice, that were initially used as **null** control group. After 6 days, the mice were sacrificed, and samples of their tissues were placed in corn oil and observed with fluorescent confocal microscopy. Although we did not detect any secondary depots in any organs (possibly due to low intensity of signal, the signal may be diffused over the entire organ), we observed major signal in samples of a thigh muscle (**Figure 19**). The signal was accumulated in a few hotspots (possibly endosomes of fibroblasts or macrophages), but diffuse fluorescence can be seen throughout the entire muscle.

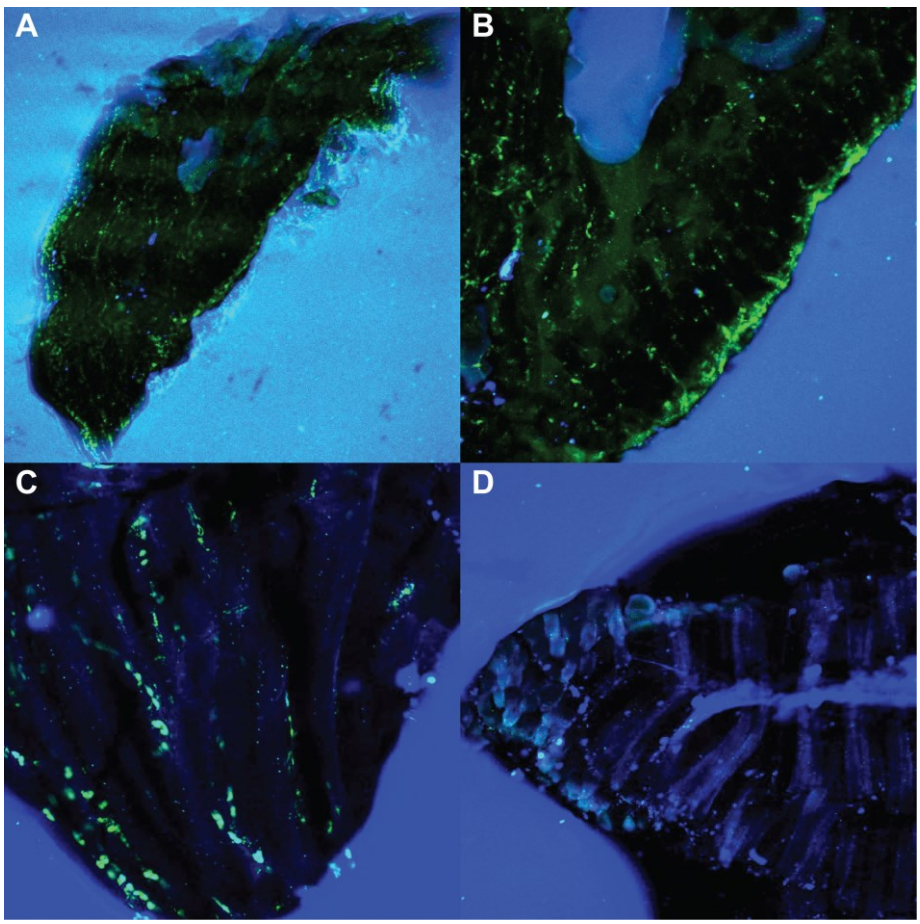

Figure 23. Fluorescence confocal micrographs of injected muscle; magnified 4-fold (**A**), 10-fold (**B**), 20-fold (**C**); and control muscle, magnified 20-fold (**D**).

5. Conclusions

We synthesized and thoroughly characterized four different thermoresponsive polyacrylamides in three different molar weights and with low dispersity indexes. Then, we investigated physico-chemical properties of these polymers in various physiologically relevant media and their biodistribution after intramuscular administration in mice.

The cloud point temperature (T_{CP}) of thermoresponsive polyacrylamides is considerably lower in physiologically relevant solvents (PBS and FBS) than in water. In particular, FBS proteins stabilize LCST polymer aggregates, but the effect of FBS proteins on T_{CP} depends on polymer concentration. At high polymer concentrations, proteins decrease the T_{CP} by competing for solvation. At low polymer concentrations, by contrast, proteins form complexes with the polymers, thus increasing aggregation. However, proteins have limited polymer-binding capacities, so their effect decreases with the increase in concentration. In turn, PBS promotes aggregation in thermoresponsive polymers by decreasing their solvation shell. Overall, our results suggest that thermoresponsive polymers with a high potential for biomedical applications should be characterized (i) by DLS for accurate T_{CP} determination and (ii) in physiologically relevant solutions rather than in pure water because they may be otherwise discarded merely for their unsuitable LCST behaviour in water. Moreover, our findings may enable us to better predict the biological properties of thermoresponsive polymers *in vivo* based on their T_{CP}. Therefore, these results may be used to optimise polymeric drug delivery systems for *in vivo* applications through *in vitro* studies.

Additionally, we determined the pharmacokinetics of dissolution of intramuscularly administered acrylamides and formulated a physiological model. Upon the administration, the depot matures for 3 to 10 days: the depot enlarges, and a portion of the polymer binds to tissues, while the rest of the administered polymer is eliminated relatively quickly. Furthermore, the dissolution of tissue-bound polymer follows 1st order kinetics with biological half-life ranging from approximately 15 days to 5 months. The speed of depot dissolution is specific for a given polymer: it roughly correlates with its T_{CP} and is only slightly increased by the polymers' molar mass. Additionally, the eliminated polymer can accumulate in liver and kidneys and thus form secondary depots in these organs. Lastly, the study polymers did not cause any local or generalized signs of pathologies or toxicity to the mice. Our results may be used to tune the biological retention of polymer in the organism to meet the demands of various biomedical applications.

6. References

(1) Kolouchová, K.; Lobaz, V.; Beneš, H.; Rosa, V. R. de la; Babuka, D.; Švec, P.; Černoch, P.; Hrubý, M.; Hoogenboom, R.; Štěpánek, P.; Groborz, O. Thermoresponsive Properties of Polyacrylamides in Physiological Solutions. *Polym. Chem.* **2021**. https://doi.org/10.1039/d1py00843a.

(2) Groborz, O.; Kolouchová, K.; Pankrác, J.; Keša, P.; Krunclová, T.; Kadlec, J.; Pierzynová, A.; Šrámek, J.; Hovořáková, M.; Dalecká, L.; Kučera, T.; Hoogenboom, R.; Hrubý, M. Pharmacokinetics of Intramuscularly Administered Thermoresponsive Polyacrylamides. **In preparation**.

(3) Szwarc, M. 'Living' Polymers. *Nature* **1956**, *178* (4543), 1168–1169. https://doi.org/10.1038/1781168a0.

(4) Jenkins, A. D.; Kratochvíl, P.; Stepto, R. F. T.; Suter, U. W. Glossary of basic terms in polymer science (IUPAC Recommendations 1996). *Pure and Applied Chemistry* **1996**, *68* (12), 2287–2311. https://doi.org/10.1351/pac199668122287.

(5) Cacioli, P.; Hawthorne, D. G.; Laslett, R. L.; Rizzardo, E.; Solomon, D. H. Copolymerization of ω-Unsaturated Oligo(Methyl Methacrylate): New Macromonomers. *J. Macromol. Sci. A J MACROMOL SCI A* **1986**, *23* (7), 839–852. https://doi.org/10.1080/00222338608069476.

(6) Aseyev, V.; Tenhu, H.; Winnik, F. M. Non-Ionic Thermoresponsive Polymers in Water. In *Self Organized Nanostructures of Amphiphilic Block Copolymers II*; Müller, A. H. E., Borisov, O., Eds.; Advances in Polymer Science; Springer Berlin Heidelberg: Berlin, Heidelberg, 2010; Vol. 242, pp 29–89. https://doi.org/10.1007/12_2010_57.

(7) Weber, C.; Hoogenboom, R.; Schubert, U. S. Temperature Responsive Bio-Compatible Polymers Based on Poly(Ethylene Oxide) and Poly(2-Oxazoline)s. *Progress in Polymer Science* **2012**, *37* (5), 686–714. https://doi.org/10.1016/j.progpolymsci.2011.10.002.

(8) Halperin, A.; Kröger, M.; Winnik, F. M. Poly(*N*-Isopropylacrylamide) Phase Diagrams: Fifty Years of Research. *Angew. Chem. Int. Ed.* **2015**, *54* (51), 15342–15367. https://doi.org/10.1002/anie.201506663.

(9) Ieong, N. S.; Hasan, M.; Phillips, D. J.; Saaka, Y.; O'Reilly, R. K.; Gibson, M. I. Polymers with Molecular Weight Dependent LCSTs Are Essential for Cooperative Behaviour. *Polym. Chem.* **2012**, *3* (3), 794–799. https://doi.org/10.1039/C2PY00604A.

(10) Lessard, D. G.; Ousalem, M.; Zhu, X. X. Effect of the Molecular Weight on the Lower Critical Solution Temperature of Poly(*N*,*N*-Diethylacrylamide) in Aqueous Solutions. *Can. J. Chem.* **2001**, *79* (12), 1870–1874. https://doi.org/10.1139/v01-180.

(11) Li, Q.; Constantinou, A. P.; Georgiou, T. K. A Library of Thermoresponsive PEG-Based Methacrylate Homopolymers: How Do the Molar Mass and Number of Ethylene Glycol Groups Affect the Cloud Point? *J. Polym. Sci.* **2021**, *59* (3), 230–239. https://doi.org/10.1002/pol.20200720.

(12) Fujishige, S.; Kubota, K.; Ando, I. Phase Transition of Aqueous Solutions of Poly(*N*-Isopropylacrylamide) and Poly(*N*-Isopropylmethacrylamide). *J. Phys. Chem.* **1989**, *93* (8), 3311–3313. https://doi.org/10.1021/j100345a085.

(13) Kolouchova, K.; Jirak, D.; Groborz, O.; Sedlacek, O.; Ziolkowska, N.; Vit, M.; Sticova, E.; Galisova, A.; Svec, P.; Trousil, J.; Hajek, M.; Hruby, M. Implant-Forming Polymeric ^{19}F MRI-Tracer with Tunable Dissolution. *J. Control. Release* **2020**, *327*, 50–60. https://doi.org/10.1016/j.jconrel.2020.07.026.

(14) Pei, Y.; Chen, J.; Yang, L.; Shi, L.; Tao, Q.; Hui, B.; Li, J. The Effect of pH on the LCST of Poly(*N*-Isopropylacrylamide) and Poly(*N*-Isopropylacrylamide-*co*-Acrylic

Acid). *J. Biomater. Sci. Polym. Ed.* **2004**, *15* (5), 585–594. https://doi.org/10.1163/156856204323046852.
(15) Pietsch, C.; Hoogenboom, R.; Schubert, U. S. Soluble Polymeric Dual Sensor for Temperature and pH Value. *Angew. Chem. Int. Ed.* **2009**, *48* (31), 5653–5656. https://doi.org/10.1002/anie.200901071.
(16) Hiruta, Y.; Nagumo, Y.; Suzuki, Y.; Funatsu, T.; Ishikawa, Y.; Kanazawa, H. The Effects of Anionic Electrolytes and Human Serum Albumin on the LCST of Poly(*N*-Isopropylacrylamide)-Based Temperature-Responsive Copolymers. *Colloids Surf. B: Biointerfaces* **2015**, *132*, 299–304. https://doi.org/10.1016/j.colsurfb.2015.05.032.
(17) Zhang, Y.; Furyk, S.; Sagle, L. B.; Cho, Y.; Bergbreiter, D. E.; Cremer, P. S. Effects of Hofmeister Anions on the LCST of PNIPAM as a Function of Molecular Weight. *J. Phys. Chem. C* **2007**, *111* (25), 8916–8924. https://doi.org/10.1021/jp0690603.
(18) Freitag, R.; Garret-Flaudy, F. Salt Effects on the Thermoprecipitation of Poly-(*N*-Isopropylacrylamide) Oligomers from Aqueous Solution. *Langmuir* **2002**, *18* (9), 3434–3440. https://doi.org/10.1021/la0106440.
(19) Zhang, Y.; Furyk, S.; Bergbreiter, D. E.; Cremer, P. S. Specific Ion Effects on the Water Solubility of Macromolecules: PNIPAM and the Hofmeister Series. *J. Am. Chem. Soc.* **2005**, *127* (41), 14505–14510. https://doi.org/10.1021/ja0546424.
(20) Skrabania, K.; Kristen, J.; Laschewsky, A.; Akdemir, O.; Hoth, A.; Lutz, J.-F. Design, Synthesis, and Aqueous Aggregation Behavior of Nonionic Single and Multiple Thermoresponsive Polymers. *Langmuir* **2007**, *23* (1), 84–93. https://doi.org/10.1021/la061509w.
(21) Judah, H. L.; Liu, P.; Zarbakhsh, A.; Resmini, M. Influence of Buffers, Ionic Strength, and PH on the Volume Phase Transition Behavior of Acrylamide-Based Nanogels. *Polymers* **2020**, *12* (11), 2590. https://doi.org/10.3390/polym12112590.
(22) Otulakowski, Ł.; Kasprów, M.; Strzelecka, A.; Dworak, A.; Trzebicka, B. Thermal Behaviour of Common Thermoresponsive Polymers in Phosphate Buffer and in Its Salt Solutions. *Polymers* **2021**, *13* (1), 90. https://doi.org/10.3390/polym13010090.
(23) Bloksma, M. M.; Bakker, D. J.; Weber, C.; Hoogenboom, R.; Schubert, U. S. The Effect of Hofmeister Salts on the LCST Transition of Poly(2-Oxazoline)s with Varying Hydrophilicity. *Macromol. Rapid Commun.* **2010**, *31* (8), 724–728. https://doi.org/10.1002/marc.200900843.
(24) Magnusson, J. P.; Khan, A.; Pasparakis, G.; Saeed, A. O.; Wang, W.; Alexander, C. Ion-Sensitive "Isothermal" Responsive Polymers Prepared in Water. *J. Am. Chem. Soc.* **2008**, *130* (33), 10852–10853. https://doi.org/10.1021/ja802609r.
(25) Zhu, X.; Gu, X.; Zhang, L.; Kong, X.-Z. Preparation and Characterization of Nanosized P(NIPAM-MBA) Hydrogel Particles and Adsorption of Bovine Serum Albumin on Their Surface. *Nanoscale Res. Lett.* **2012**, *7* (1), 519. https://doi.org/10.1186/1556-276X-7-519.
(26) Trongsatitkul, T.; Budhlall, B. M. Temperature Dependence of Serum Protein Adsorption in PEGylated PNIPAm Microgels. *Colloids Surf. B: Biointerfaces* **2013**, *103*, 244–252. https://doi.org/10.1016/j.colsurfb.2012.10.053.
(27) Bebis, K.; W. Jones, M.; M. Haddleton, D.; I. Gibson, M. Thermoresponsive Behaviour of Poly[(Oligo(Ethyleneglycol Methacrylate)]s and Their Protein Conjugates: Importance of Concentration and Solvent System. *Polym. Chem.* **2011**, *2* (4), 975–982. https://doi.org/10.1039/C0PY00408A.
(28) Okada, Y.; Tanaka, F. Cooperative Hydration, Chain Collapse, and Flat LCST Behavior in Aqueous Poly(*N*-Isopropylacrylamide) Solutions. *Macromolecules* **2005**, *38* (10), 4465–4471. https://doi.org/10.1021/ma0502497.

(29) Ellis, R. J. Macromolecular Crowding: Obvious but Underappreciated. *Trends Biochem. Sci.* **2001**, *26* (10), 597–604. https://doi.org/10.1016/S0968-0004(01)01938-7.
(30) Suzuki, S.; Sawada, T.; Ishizone, T.; Serizawa, T. Affinity-Based Thermoresponsive Precipitation of Proteins Modified with Polymer-Binding Peptides. *Chem. Commun.* **2016**, *52* (33), 5670–5673. https://doi.org/10.1039/C6CC00594B.
(31) Jochum, F. D.; Theato, P. Temperature- and Light-Responsive Smart Polymer Materials. *Chem. Soc. Rev.* **2013**, *42* (17), 7468–7483. https://doi.org/10.1039/C2CS35191A.
(32) Ray, B.; Okamoto, Y.; Kamigaito, M.; Sawamoto, M.; Seno, K.; Kanaoka, S.; Aoshima, S. Effect of Tacticity of Poly(*N*-Isopropylacrylamide) on the Phase Separation Temperature of Its Aqueous Solutions. *Polym. J.* **2005**, *37* (3), 234–237. https://doi.org/10.1295/polymj.37.234.
(33) Hrubý, M.; Šubr, V.; Kučka, J.; Kozempel, J.; Lebeda, O.; Sikora, A. Thermoresponsive Polymers as Promising New Materials for Local Radiotherapy. *Appl. Radiat. Isot.* **2005**, *63* (4), 423–431. https://doi.org/10.1016/j.apradiso.2005.05.043.
(34) Xia, Y.; Burke, N. A. D.; Stöver, H. D. H. End Group Effect on the Thermal Response of Narrow-Disperse Poly(*N*-Isopropylacrylamide) Prepared by Atom Transfer Radical Polymerization. *Macromolecules* **2006**, *39* (6), 2275–2283. https://doi.org/10.1021/ma0519617.
(35) Cao, G.; Li, G.; Yang, Q.; Liu, Z.; Liu, Z.; Jiang, J. LCST-Type Hyperbranched Poly(Oligo(Ethylene Glycol) with Thermo- and CO_2 -Responsive Backbone. *Macromol. Rapid Commun.* **2018**, *39* (6), 1700684. https://doi.org/10.1002/marc.201700684.
(36) Panayiotou, C.; Sanchez, I. C. Hydrogen Bonding in Fluids: An Equation-of-State Approach. *J. Phys. Chem.* **1991**, *95* (24), 10090–10097. https://doi.org/10.1021/j100177a086.
(37) Afroze, F.; Nies, E.; Berghmans, H. Phase Transitions in the System Poly(*N*-Isopropylacrylamide)/Water and Swelling Behaviour of the Corresponding Networks. *J. Mol. Struct.* **2000**, *554* (1), 55–68. https://doi.org/10.1016/S0022-2860(00)00559-7.
(38) Rebelo, L. P. N.; Visak, Z. P.; de Sousa, H. C.; Szydlowski, J.; Gomes de Azevedo, R.; Ramos, A. M.; Najdanovic-Visak, V.; Nunes da Ponte, M.; Klein, J. Double Critical Phenomena in (Water + Polyacrylamides) Solutions. *Macromolecules* **2002**, *35* (5), 1887–1895. https://doi.org/10.1021/ma011533a.
(39) Zhao, C.; Ma, Z.; Zhu, X. X. Rational Design of Thermoresponsive Polymers in Aqueous Solutions: A Thermodynamics Map. *Prog. Polym. Sci.* **2019**, *90*, 269–291. https://doi.org/10.1016/j.progpolymsci.2019.01.001.
(40) Heyda, J.; Dzubiella, J. Thermodynamic Description of Hofmeister Effects on the LCST of Thermosensitive Polymers. *J. Phys. Chem. B* **2014**, *118* (37), 10979–10988. https://doi.org/10.1021/jp5041635.
(41) Chang, B. H.; Bae, Y. C. Liquid–Liquid Equilibria of Binary Polymer Solutions with Specific Interactions. *Polymer* **1998**, *39* (25), 6449–6454. https://doi.org/10.1016/S0032-3861(97)10386-X.
(42) Zhang, Q.; Weber, C.; Schubert, U. S.; Hoogenboom, R. Thermoresponsive Polymers with Lower Critical Solution Temperature: From Fundamental Aspects and Measuring Techniques to Recommended Turbidimetry Conditions. *Mater. Horiz.* **2017**, *4* (2), 109–116. https://doi.org/10.1039/C7MH00016B.
(43) Boutris, C.; Chatzi, E. G.; Kiparissides, C. Characterization of the LCST Behaviour of Aqueous Poly(*N*-Isopropylacrylamide) Solutions by Thermal and Cloud Point

Techniques. *Polymer* **1997**, *38* (10), 2567–2570. https://doi.org/10.1016/S0032-3861(97)01024-0.
(44) Štěpánek, P. Chapter 4: Data Analysis in Dynamic Light Scattering. In *Dynamic Light Scattering*; Brown, W., Ed.; Clarendon Press: Oxford, 1993; p 760.
(45) Schild, H. G.; Tirrell, D. A. Microcalorimetric Detection of Lower Critical Solution Temperatures in Aqueous Polymer Solutions. *J. Phys. Chem.* **1990**, *94* (10), 4352–4356. https://doi.org/10.1021/j100373a088.
(46) Otake, K.; Inomata, H.; Konno, M.; Saito, S. Thermal Analysis of the Volume Phase Transition with *N*-Isopropylacrylamide Gels. *Macromolecules* **1990**, *23* (1), 283–289. https://doi.org/10.1021/ma00203a049.
(47) Ward, M. A.; Georgiou, T. K. Thermoresponsive Polymers for Biomedical Applications. *Polymers* **2011**, *3* (3), 1215–1242. https://doi.org/10.3390/polym3031215.
(48) Wu, D.-Q.; Zhu, J.; Han, H.; Zhang, J.-Z.; Wu, F.-F.; Qin, X.-H.; Yu, J.-Y. Synthesis and Characterization of Arginine-NIPAAm Hybrid Hydrogel as Wound Dressing: *In Vitro* and *in Vivo* Study. *Acta Biomater.* **2018**, *65*, 305–316. https://doi.org/10.1016/j.actbio.2017.08.048.
(49) Elloumi-Hannachi, I.; Yamato, M.; Okano, T. Cell Sheet Engineering: A Unique Nanotechnology for Scaffold-Free Tissue Reconstruction with Clinical Applications in Regenerative Medicine. *J. Intern. Med.* **2010**, *267* (1), 54–70. https://doi.org/10.1111/j.1365-2796.2009.02185.x.
(50) Liechty, W. B.; Kryscio, D. R.; Slaughter, B. V.; Peppas, N. A. Polymers for Drug Delivery Systems. *Annu. Rev. Chem. Biomol. Eng.* **2010**, *1* (1), 149–173. https://doi.org/10.1146/annurev-chembioeng-073009-100847.
(51) Hatefi, A.; Amsden, B. Biodegradable Injectable in Situ Forming Drug Delivery Systems. *J. Control. Release* **2002**, *80* (1), 9–28. https://doi.org/10.1016/S0168-3659(02)00008-1.
(52) Ruel-Gariépy, E.; Leroux, J.-C. In Situ-Forming Hydrogels—Review of Temperature-Sensitive Systems. *Eur. J. Pharm. Biopharm.* **2004**, *58* (2), 409–426. https://doi.org/10.1016/j.ejpb.2004.03.019.
(53) Sedláček, O.; Černoch, P.; Kučka, J.; Konefal, R.; Štěpánek, P.; Vetrík, M.; Lodge, T. P.; Hrubý, M. Thermoresponsive Polymers for Nuclear Medicine: Which Polymer Is the Best? *Langmuir* **2016**, *32* (24), 6115–6122. https://doi.org/10.1021/acs.langmuir.6b01527.
(54) Hrubý, M.; Kucka, J.; Lebeda, O.; Mackova, H.; Babič, M.; Koňák, Č.; Studenovský, M.; Síkora, A.; Kozempel, J.; Ulbrich, K. New Bioerodable Thermoresponsive Polymers for Possible Radiotherapeutic Applications. *J. Control. Release* **2007**, *119* (1), 25–33. https://doi.org/10.1016/j.jconrel.2007.02.009.
(55) Yang, L.; Fan, X.; Zhang, J.; Ju, J. Preparation and Characterization of Thermoresponsive Poly(N-Isopropylacrylamide) for Cell Culture Applications. *Polymers* **2020**, *12* (2), 389. https://doi.org/10.3390/polym12020389.
(56) Yamada, N.; Okano, T.; Sakai, H.; Karikusa, F.; Sawasaki, Y.; Sakurai, Y. Thermo-Responsive Polymeric Surfaces; Control of Attachment and Detachment of Cultured Cells. *Die Makromolekulare Chemie, Rapid Communications* **1990**, *11* (11), 571–576. https://doi.org/10.1002/marc.1990.030111109.
(57) Ekerdt, B. L.; Fuentes, C. M.; Lei, Y.; Adil, M. M.; Ramasubramanian, A.; Segalman, R. A.; Schaffer, D. V. Thermoreversible Hyaluronic Acid-PNIPAAm Hydrogel Systems for 3D Stem Cell Culture. *Adv. Healthc. Mater.* **2018**, *7* (12), 1800225. https://doi.org/10.1002/adhm.201800225.

(58) Okano, T.; Yamada, N.; Okuhara, M.; Sakai, H.; Sakurai, Y. Mechanism of Cell Detachment from Temperature-Modulated, Hydrophilic- Hydrophobic Polymer Surfaces. *Biomaterials* **1995**, *16* (4), 7.

(59) Kolouchova, K.; Groborz, O.; Svec, P.; Starcuk, Z.; Slouf, M.; Hruby, M. Thermo- and ROS-Responsive Self-Assembled Polymer Nanoparticle Tracers for ^{19}F MRI Theranostics. *Biomacromolecules* **2021**, *22* (6), 2325–2337. https://doi.org/10.1021/acs.biomac.0c01316.

(60) Alhoranta, A. M.; Lehtinen, J. K.; Urtti, A. O.; Butcher, S. J.; Aseyev, V. O.; Tenhu, H. J. Cationic Amphiphilic Star and Linear Block Copolymers: Synthesis, Self-Assembly, and *in Vitro* Gene Transfection. *Biomacromolecules* **2011**, *12* (9), 3213–3222. https://doi.org/10.1021/bm2006906.

(61) Lavigne, M. D.; Pennadam, S. S.; Ellis, J.; Yates, L. L.; Alexander, C.; Górecki, D. C. Enhanced Gene Expression through Temperature Profile-Induced Variations in Molecular Architecture of Thermoresponsive Polymer Vectors. *J. Gene Med.* **2007**, *9* (1), 44–54. https://doi.org/10.1002/jgm.992.

(62) Ganta, S.; Devalapally, H.; Shahiwala, A.; Amiji, M. A Review of Stimuli-Responsive Nanocarriers for Drug and Gene Delivery. *J. Control. Release* **2008**, *126* (3), 187–204. https://doi.org/10.1016/j.jconrel.2007.12.017.

(63) Doberenz, F.; Zeng, K.; Willems, C.; Zhang, K.; Groth, T. Thermoresponsive Polymers and Their Biomedical Application in Tissue Engineering – a Review. *J. Mater. Chem. B* **2020**, *8* (4), 607–628. https://doi.org/10.1039/C9TB02052G.

(64) Lee, K. Y.; Mooney, D. J. Hydrogels for Tissue Engineering. *Chem. Rev.* **2001**, *101* (7), 1869–1880. https://doi.org/10.1021/cr000108x.

(65) Van Vlierberghe, S.; Dubruel, P.; Schacht, E. Biopolymer-Based Hydrogels As Scaffolds for Tissue Engineering Applications: A Review. *Biomacromolecules* **2011**, *12* (5), 1387–1408. https://doi.org/10.1021/bm200083n.

(66) Wei, Y.; Zeng, Q.; Hu, Q.; Wang, M.; Tao, J.; Wang, L. Self-Cleaned Electrochemical Protein Imprinting Biosensor Basing on a Thermo-Responsive Memory Hydrogel. *Biosens. Bioelectron.* **2018**, *99*, 136–141. https://doi.org/10.1016/j.bios.2017.07.049.

(67) Pacifici, N.; Bolandparvaz, A.; Lewis, J. S. Stimuli-Responsive Biomaterials for Vaccines and Immunotherapeutic Applications. *Adv. Therap.* **2020**, *3* (11), 2000129. https://doi.org/10.1002/adtp.202000129.

(68) Ayano, E.; Kanazawa, H. Aqueous Chromatography System Using Temperature-Responsive Polymer-Modified Stationary Phases. *J. Sep. Sci.* **2006**, *29* (6), 738–749. https://doi.org/10.1002/jssc.200500485.

(69) Bergbreiter, D. E. Using Soluble Polymers To Recover Catalysts and Ligands. *Chem. Rev.* **2002**, *102* (10), 3345–3384. https://doi.org/10.1021/cr010343v.

(70) Kučka, J.; Hrubý, M.; Lebeda, O. Biodistribution of a Radiolabelled Thermoresponsive Polymer in Mice. *Appl. Radiat. Isot.* **2010**, *68* (6), 1073–1078. https://doi.org/10.1016/j.apradiso.2010.01.022.

(71) Bertrand, N.; Fleischer, J. G.; Wasan, K. M.; Leroux, J.-C. Pharmacokinetics and Biodistribution of *N*-Isopropylacrylamide Copolymers for the Design of pH-Sensitive Liposomes. *Biomaterials* **2009**, *30* (13), 2598–2605. https://doi.org/10.1016/j.biomaterials.2008.12.082.

(72) Harris, R. K.; Becker, E. D.; Goodfellow, R.; Granger, P. (IUPAC Recommendations 2001). *Pure and Applied Chemistry* **2001**, 24.

(73) Harris, R. K.; Becker, E. D.; Cabral de Menezes, S. M.; Granger, P.; Hoffman, R. E.; Zilm, K. W. Further Conventions for NMR Shielding and Chemical Shifts (IUPAC Recommendations 2008). *Pure and Applied Chemistry* **2008**, *80* (1), 59–84. https://doi.org/10.1351/pac200880010059.

(74) Dračínský, M. *NMR spektroskopie pro chemiky*, 1st ed.; Přírodovědecká fakulta, UK: Prague, 2021.
(75) Roy Hoffman lab. Multinuclear NMR http://chem.ch.huji.ac.il/nmr/techniques/1d/multi.html (accessed 2021 -07 -16).
(76) McNaught, A. D.; Wilkinson, A. *IUPAC. Compendium of Chemical Terminology*, 2nd ed.; Blackwell Scientific Publications: Oxford, 1997.
(77) Serdyuk, I. N.; Zaccai, N. R.; Zaccai, J.; Zaccai, G. *Methods in Molecular Biophysics*; Cambridge University Press, 2017.
(78) Ritter, A.; Schmid, M.; Affolter, S. Determination of Molecular Weights by Size Exclusion Chromatography (SEC) – Results of Round Robin Tests. *Polymer Testing* **2010**, *29* (8), 945–952. https://doi.org/10.1016/j.polymertesting.2010.08.002.
(79) Kim, C.; Deratani, A.; Bonfils, F. Determination of the Refractive Index Increment of Natural and Synthetic Poly(Cis-1,4-Isoprene) Solutions and Its Effect on Structural Parameters. *J. Liq. Chromatogr. Relat. Technol.* **2009**, *33* (1), 37–45. https://doi.org/10.1080/10826070903427072.
(80) Waters 2410 Differential Refractometer Operator's Guide, Revision 2. Waters 2021.
(81) Babuka, D.; Kolouchová, K.; Groborz, O.; Tošner, Z.; Zhigunov, A.; Štěpánek, P.; Hrubý, M. Internal Structure of Thermoresponsive Physically Crosslinked Nanogel of Poly[*N*-(2-Hydroxypropyl)Methacrylamide]-Block-Poly[*N*-(2,2-Difluoroethyl)Acrylamide], Prominent ^{19}F MRI Tracer. *Nanomaterials* **2020**, *10* (11), 2231. https://doi.org/10.3390/nano10112231.
(82) Babuka, D.; Kolouchova, K.; Hruby, M.; Groborz, O.; Tosner, Z.; Zhigunov, A.; Stepanek, P. Investigation of the Internal Structure of Thermoresponsive Diblock Poly(2-Methyl-2-Oxazoline)-*b*-Poly[N-(2,2-Difluoroethyl)Acrylamide] Copolymer Nanoparticles. *Eur. Polym. J.* **2019**, *121*, 109306. https://doi.org/10.1016/j.eurpolymj.2019.109306.
(83) Kolouchova, K.; Sedlacek, O.; Jirak, D.; Babuka, D.; Blahut, J.; Kotek, J.; Vit, M.; Trousil, J.; Konefał, R.; Janouskova, O.; Podhorska, B.; Slouf, M.; Hruby, M. Self-Assembled Thermoresponsive Polymeric Nanogels for ^{19}F MR Imaging. *Biomacromolecules* **2018**, *19* (8), 3515–3524. https://doi.org/10.1021/acs.biomac.8b00812.
(84) Carvalho, P. M.; Felício, M. R.; Santos, N. C.; Gonçalves, S.; Domingues, M. M. Application of Light Scattering Techniques to Nanoparticle Characterization and Development. *Front. Chem.* **2018**, *0*. https://doi.org/10.3389/fchem.2018.00237.
(85) Chu, B. *Laser Light Scattering*; Elsevier, 1974.
(86) The principles of dynamic light scattering :: Anton Paar Wiki https://wiki.anton-paar.com/cz-cs/principy-dynamickeho-rozptylu-svetla/ (accessed 2021 -07 -16).
(87) Provencher, S. W. CONTIN: A General Purpose Constrained Regularization Program for Inverting Noisy Linear Algebraic and Integral Equations. *Comput. Phys. Commun.* **1982**, *27* (3), 229–242. https://doi.org/10.1016/0010-4655(82)90174-6.
(88) Provencher, S. W. A Constrained Regularization Method for Inverting Data Represented by Linear Algebraic or Integral Equations. *Comput. Phys. Commun.* **1982**, *27* (3), 213–227. https://doi.org/10.1016/0010-4655(82)90173-4.
(89) Pierce, M. M.; Raman, C. S.; Nall, B. T. Isothermal Titration Calorimetry of Protein–Protein Interactions. *Methods* **1999**, *19* (2), 213–221. https://doi.org/10.1006/meth.1999.0852.
(90) Wiseman, T.; Williston, S.; Brandts, J. F.; Lin, L.-N. Rapid Measurement of Binding Constants and Heats of Binding Using a New Titration Calorimeter. *Anal. Biochem.* **1989**, *179* (1), 131–137. https://doi.org/10.1016/0003-2697(89)90213-3.

(91) ISO 10993-5:2009 Biological Evaluation of Medical Devices — Part 5: Tests for in Vitro Cytotoxicity. International Organisation for Standardization June 2009.
(92) Mosmann, T. Rapid Colorimetric Assay for Cellular Growth and Survival: Application to Proliferation and Cytotoxicity Assays. *Journal of Immunological Methods* **1983**, *65* (1), 55–63. https://doi.org/10.1016/0022-1759(83)90303-4.
(93) Stockert, J. C.; Blázquez-Castro, A.; Cañete, M.; Horobin, R. W.; Villanueva, Á. MTT Assay for Cell Viability: Intracellular Localization of the Formazan Product Is in Lipid Droplets. *Acta Histochem.* **2012**, *114* (8), 785–796. https://doi.org/10.1016/j.acthis.2012.01.006.
(94) Twigg, R. S. Oxidation-Reduction Aspects of Resazurin. *Nature* **1945**, *155* (3935), 401–402. https://doi.org/10.1038/155401a0.
(95) O'Brien, J.; Wilson, I.; Orton, T.; Pognan, F. Investigation of the Alamar Blue (Resazurin) Fluorescent Dye for the Assessment of Mammalian Cell Cytotoxicity. *Eur. J. Biochem.* **2000**, *267* (17), 5421–5426. https://doi.org/10.1046/j.1432-1327.2000.01606.x.
(96) Suresh, K. B.; Gerald, T. M.; Liang-Shang, G.; Jing-Tao, W.; Frank, W. L. Strategy of Utilizing In Vitro and In Vivo ADME Tools for Lead Optimization and Drug Candidate Selection. *Current Topics in Medicinal Chemistry* **2005**, *5* (11), 1033–1038.
(97) Hartinger, C. G.; Jakupec, M. A.; Zorbas-Seifried, S.; Groessl, M.; Egger, A.; Berger, W.; Zorbas, H.; Dyson, P. J.; Keppler, B. K. KP1019, A New Redox-Active Anticancer Agent – Preclinical Development and Results of a Clinical Phase I Study in Tumor Patients. *Chem. Biodivers.* **2008**, *5* (10), 2140–2155. https://doi.org/10.1002/cbdv.200890195.
(98) Le Blanc, S.; Garrick, M. D.; Arredondo, M. Heme Carrier Protein 1 Transports Heme and Is Involved in Heme-Fe Metabolism. *American Journal of Physiology-Cell Physiology* **2012**, *302* (12), C1780–C1785. https://doi.org/10.1152/ajpcell.00080.2012.
(99) Wright, E. M.; Hirayama, B. A.; Loo, D. F. Active Sugar Transport in Health and Disease. *Journal of Internal Medicine* **2007**, *261* (1), 32–43. https://doi.org/10.1111/j.1365-2796.2006.01746.x.
(100) Moor, M. J.; Steiner, S. H.; Jachertz, G.; Bickel, M. H. Adipose Tissue Distribution and Chemical Structure of Basic Lipophilic Drugs: Desipramine, N-Acetyl Desipramine, and Haloperidol. *Pharmacol. Toxicol.* **1992**, *70* (2), 121–124. https://doi.org/10.1111/j.1600-0773.1992.tb00440.x.
(101) Vandenbossche, J.; Huisman, M.; Xu, Y.; Sanderson-Bongiovanni, D.; Soons, P. Loperamide and P-Glycoprotein Inhibition: Assessment of the Clinical Relevance. *J. Pharm. Pharmacol.* **2010**, *62* (4), 401–412. https://doi.org/10.1211/jpp.62.04.0001.
(102) Newberg, A.; Alavi, A.; Reivich, M. Determination of Regional Cerebral Function with FDG-PET Imaging in Neuropsychiatric Disorders. *Semin. Nucl. Med.* **2002**, *32* (1), 13–34. https://doi.org/10.1053/snuc.2002.29276.
(103) Švec, P.; Nový, Z.; Kučka, J.; Petřík, M.; Sedláček, O.; Kuchař, M.; Lišková, B.; Medvedíková, M.; Kolouchová, K.; Groborz, O.; Loukotová, L.; Konefał, R. Ł.; Hajdúch, M.; Hrubý, M. Iodinated Choline Transport-Targeted Tracers. *J. Med. Chem.* **2020**, *63* (24), 15960–15978. https://doi.org/10.1021/acs.jmedchem.0c01710.
(104) Dean, M.; Hamon, Y.; Chimini, G. The Human ATP-Binding Cassette (ABC) Transporter Superfamily. *J. Lipid Res.* **2001**, *42* (7), 1007–1017. https://doi.org/10.1016/S0022-2275(20)31588-1.
(105) Guengerich, F. P. Common and Uncommon Cytochrome P450 Reactions Related to Metabolism and Chemical Toxicity. *Chem. Res. Toxicol.* **2001**, *14* (6), 611–650. https://doi.org/10.1021/tx0002583.

(106) Liston, H. L.; Markowitz, J. S.; DeVane, C. L. Drug Glucuronidation in Clinical Psychopharmacology. *J. Clin. Psychopharmacol* **2001**, *21* (5), 500–515.
(107) Hunter, F. T.; Mudd, S. G. Carbon Dioxide Treatment in Acute Alcoholic Intoxication: Preliminary Report. *N. Engl. J. Med.* **1924**, *190* (23), 971–974. https://doi.org/10.1056/NEJM192406051902303.
(108) Assessment, U. E. N. C. for E.; Soto, V. IRIS Toxicological Review of Benzene (Noncancer Effects) https://cfpub.epa.gov/ncea/risk/recordisplay.cfm?deid=51760 (accessed 2021 -07 -16).
(109) Brodie, B. B.; Axelrod, J. The Estimation of Acetanilide and Its Metabolic Products, Aniline, N-Acetyl p-Aminophenol and p-Amino-Phenol, Free and Total Conjugated, in Biological Fluids and Tissues. *J. Pharmacol. Exp. Ther.* **1948**, *94* (1), 22–28.
(110) Groborz, O.; Poláková, L.; Kolouchová, K.; Švec, P.; Loukotová, L.; Miriyala, V. M.; Francová, P.; Kučka, J.; Krijt, J.; Páral, P.; Báječný, M.; Heizer, T.; Pohl, R.; Dunlop, D.; Czernek, J.; Šefc, L.; Beneš, J.; Štěpánek, P.; Hobza, P.; Hrubý, M. Chelating Polymers for Hereditary Hemochromatosis Treatment. *Macromol. Biosci.* **2020**, *20* (12), 2000254. https://doi.org/10.1002/mabi.202000254.
(111) Groborz, O. Chelating Polymers for the Haemochromatosis Treatment. Bakalářská práce, Charles University, Department of Inorganic Chemistry, 2019, http://hdl.handle.net/20.500.11956/108596
(112) Hála, J. *Radioaktivní izotopy*; 1; Sursum: Tišnov, 2013.
(113) Chu, S. Y. F.; L.P. Ekström; Firestone, R. B. The Lund/LBNL Nuclear Data Search http://nucleardata.nuclear.lu.se/toi/.
(114) Rizk, T. H.; Nagalli, S. Technetium (99mTc) Sestamibi. In *StatPearls*; StatPearls Publishing: Treasure Island (FL), 2021.
(115) Moretti, J.-L.; Defer, G.; Cinotti, L.; Cesaro, P.; Degos, J.-D.; Vigneron, N.; Ducassou, D.; Holman, B. L. "Luxury Perfusion" With99mTc-HMPAO And123I-IMP SPECT Imaging during the Subacute Phase of Stroke. *Eur J Nucl Med* **1990**, *16* (1), 17–22. https://doi.org/10.1007/BF01566007.
(116) Jirak, D.; Galisova, A.; Kolouchova, K.; Babuka, D.; Hruby, M. Fluorine Polymer Probes for Magnetic Resonance Imaging: Quo Vadis? *Magn Reson Mater Phy* **2019**, *32* (1), 173–185. https://doi.org/10.1007/s10334-018-0724-6.
(117) Geraldes, C. F. G. C.; Laurent, S. Classification and Basic Properties of Contrast Agents for Magnetic Resonance Imaging. *Contrast Media & Molecular Imaging* **2009**, *4* (1), 1–23. https://doi.org/10.1002/cmmi.265.
(118) European Commission. Directorate General for Health and Consumers. *Health Effects of Artificial Light.*; Publications Office: LU, 2012.
(119) Schleucher, J.; Schwendinger, M.; Sattler, M.; Schmidt, P.; Schedletzky, O.; Glaser, S. J.; Sørensen, O. W.; Griesinger, C. A General Enhancement Scheme in Heteronuclear Multidimensional NMR Employing Pulsed Field Gradients. *J. Biomol. NMR* **1994**, *4* (2), 301–306. https://doi.org/10.1007/BF00175254.
(120) Kay, L.; Keifer, P.; Saarinen, T. Pure Absorption Gradient Enhanced Heteronuclear Single Quantum Correlation Spectroscopy with Improved Sensitivity. *J. Am. Chem. Soc.* **1992**, *114* (26), 10663–10665. https://doi.org/10.1021/ja00052a088.
(121) Gottlieb, H. E.; Kotlyar, V.; Nudelman, A. NMR Chemical Shifts of Common Laboratory Solvents as Trace Impurities. *J. Org. Chem.* **1997**, *62* (21), 7512–7515. https://doi.org/10.1021/jo971176v.
(122) Dulbecco, R.; Vogt, M. Plaque Formation and Isolation of Pure Lines of Poliomyelitis Viruses. *J. Exp. Med.* **1954**, *99* (2), 167–182. https://doi.org/10.1084/jem.99.2.167.

(123) Jakeš, J. Regularized Positive Exponential Sum (REPES) Program - A Way of Inverting Laplace Transform Data Obtained by Dynamic Light Scattering. *Collect. Czech. Chem. Commun.* **1995**, *60* (11), 1781–1797. https://doi.org/10.1135/cccc19951781.
(124) Chiefari, J.; Chong, Y. K. (Bill); Ercole, F.; Krstina, J.; Jeffery, J.; Le, T. P. T.; Mayadunne, R. T. A.; Meijs, G. F.; Moad, C. L.; Moad, G.; Rizzardo, E.; Thang, S. H. Living Free-Radical Polymerization by Reversible Addition−Fragmentation Chain Transfer: The RAFT Process. *Macromolecules* **1998**, *31* (16), 5559–5562. https://doi.org/10.1021/ma9804951.
(125) Zhou, C.; Hillmyer, M. A.; Lodge, T. P. Micellization and Micellar Aggregation of Poly(Ethylene-*Alt*-Propylene)-*b*-Poly(Ethylene Oxide)-*b*-Poly(*N*-Isopropylacrylamide) Triblock Terpolymers in Water. *Macromolecules* **2011**, *44* (6), 1635–1641. https://doi.org/10.1021/ma102786q.
(126) Burns, J. A.; Butler, J. C.; Moran, J.; Whitesides, G. M. Selective Reduction of Disulfides by Tris(2-Carboxyethyl)Phosphine. *J. Org. Chem.* **1991**, *56* (8), 2648–2650. https://doi.org/10.1021/jo00008a014.
(127) Bak, J. M.; Lee, H. Novel Thermoresponsive Fluorinated Double-Hydrophilic Poly[*N*-(2,2-Difluoroethyl)Acrylamide]-*b*-[*N*-(2-Fluoroethyl)Acrylamide] Block Copolymers. *J. Polym. Sci., Part A-1: Polym. Chem.* **2013**, *51* (9), 1976–1982. https://doi.org/10.1002/pola.26578.
(128) Zafrani, Y.; Yeffet, D.; Sod-Moriah, G.; Berliner, A.; Amir, D.; Marciano, D.; Gershonov, E.; Saphier, S. Difluoromethyl Bioisostere: Examining the "Lipophilic Hydrogen Bond Donor" Concept. *J. Med. Chem.* **2017**, *60* (2), 797–804. https://doi.org/10.1021/acs.jmedchem.6b01691.
(129) Monnery, B. D.; Hoogenboom, R. Thermoresponsive Hydrogels Formed by Poly(2-Oxazoline) Triblock Copolymers. *Polym. Chem.* **2019**, *10* (25), 3480–3487. https://doi.org/10.1039/C9PY00300B.
(130) Wyffels, L.; Verbrugghen, T.; Monnery, B. D.; Glassner, M.; Stroobants, S.; Hoogenboom, R.; Staelens, S. MPET Imaging of the Pharmacokinetic Behavior of Medium and High Molar Mass ^{89}Zr-Labeled Poly(2-Ethyl-2-Oxazoline) in Comparison to Poly(Ethylene Glycol). *J. Control. Release* **2016**, *235*, 63–71. https://doi.org/10.1016/j.jconrel.2016.05.048.
(131) Seymour, L. W.; Duncan, R.; Strohalm, J.; Kopeček, J. Effect of Molecular Weight (Mw) of N-(2-Hydroxypropyl)Methacrylamide Copolymers on Body Distribution and Rate of Excretion after Subcutaneous, Intraperitoneal, and Intravenous Administration to Rats. *Journal of Biomedical Materials Research* **1987**, *21* (11), 1341–1358. https://doi.org/10.1002/jbm.820211106.
(132) Valk, J. van der; Bieback, K.; Buta, C.; Cochrane, B.; Dirks, W. G.; Fu, J.; Hickman, J. J.; Hohensee, C.; Kolar, R.; Liebsch, M.; Pistollato, F.; Schulz, M.; Thieme, D.; Weber, T.; Wiest, J.; Winkler, S.; Gstraunthaler, G. Fetal Bovine Serum (FBS): Past – Present – Future. *ALTEX* **2018**, *35* (1), 99–118. https://doi.org/10.14573/altex.1705101.
(133) Okur, H. I.; Hladílková, J.; Rembert, K. B.; Cho, Y.; Heyda, J.; Dzubiella, J.; Cremer, P. S.; Jungwirth, P. Beyond the Hofmeister Series: Ion-Specific Effects on Proteins and Their Biological Functions. *J. Phys. Chem. B* **2017**, *121* (9), 1997–2014. https://doi.org/10.1021/acs.jpcb.6b10797.
(134) Ross, P. D.; Rekharsky, M. V. Thermodynamics of Hydrogen Bond and Hydrophobic Interactions in Cyclodextrin Complexes. *Biophys. J.* **1996**, *71* (4), 2144–2154. https://doi.org/10.1016/S0006-3495(96)79415-8.
(135) Pestman, J. M.; Kevelam, J.; Blandamer, M. J.; van Doren, H. A.; Kellogg, R. M.; Engberts, J. B. F. N. Thermodynamics of Micellization of Nonionic Saccharide-Based

N-Acyl-*N*-Alkylaldosylamine and *N*-Acyl-*N*-Alkylamino-1-Deoxyalditol Surfactants. *Langmuir* **1999**, *15* (6), 2009–2014. https://doi.org/10.1021/la981404w.
(136) Némethy, G. Hydrophobic Interactions. *Angew. Chem. Int. Ed.* **1967**, *6* (3), 195–206. https://doi.org/10.1002/anie.196701951.
(137) Schreiner, G. F. The Mesangial Phagocyte and Its Regulation of Contractile Cell Biology. *JASN* **1992**, *2* (10), S74. https://doi.org/10.1681/ASN.V210s74.
(138) Gjedde, S. B.; Gjeode, A. Organ Blood Flow Rates and Cardiac Output of the BALB/c Mouse. *Comp. Biochem. Physiol. Part A Mol. Integr. Physiol.* **1980**, *67* (4), 671–674. https://doi.org/10.1016/0300-9629(80)90258-3.
(139) Maxie, M. G. *Jubb, Kennedy & Palmer's Pathology of Domestic Animals: Volume 3*; Elsevier Health Sciences, 2015.
(140) Tsang, A. P.; Fujiwara, Y.; Hom, D. B.; Orkin, S. H. Failure of Megakaryopoiesis and Arrested Erythropoiesis in Mice Lacking the GATA-1 Transcriptional Cofactor FOG. *Genes Dev.* **1998**, *12* (8), 1176–1188.